The plume head-lithosphere interactions near intra-continental plate boundaries

Evgenii E.B. Burov, Laurent Guillou-Frottier, Elia d'Acremont, Laetitia Le Pourhiet, Sierd Cloething

Elsevier Editorial System(tm) for Tectonophysics

Manuscript Draft

Manuscript Number: TECTO5274R1

Title: The plume head -lithosphere interactions near intra-continental plate boundaries

Article Type: Research Paper

Section/Category:

Keywords: plum-lithosphere interaction; cratons; metallogenic crises; rheology; numerical modeling

Corresponding Author: Dr. E.B. Burov,

Corresponding Author's Institution: Université Pierre et Marie Curie, Laboratoire de Tectonique

First Author: E.B. Burov

Order of Authors: E.B. Burov; Laurent Guillou-Frottier; Elia d'Acremont; Laetitia LePourhiet; Sierd Cloetingh; Sierd Cloetingh

Manuscript Region of Origin:

Abstract: Plume-lithosphere interactions (PLI) have important consequences both for tectonic and mineralogical evolution of the lithosphere: for example, Archean metallogenic crises at the boundaries of the West African and Australian cratons coincide with postulated plume events. In continents, PLI are often located near boundaries between younger plates (e.g., orogenic) and older stable plates (e.g., cratons), which represent important geometrical, thermal and rheological barriers that interact with the emplacement of the plume head (e.g., Archean West Africa, East Africa, Pannonian - Carpathian system). The observable PLI signatures are conditioned by plume dynamics but also by lithosphere rheology and structure. We address the latter problem by considering a free-surface numerical model of PLI with two stratified elasto-viscous-plastic (EVP) lithospheric plates, one of which is older and thicker than another. The results show that: (1) plume head flattening is asymmetric, it is blocked from one side by the cold vertical boundary of the

older plate, which leads to the mechanical decoupling of the crust from the mantle lithosphere, and to localized faulting at the cratonic margin; (2) the return flow from the plume head results in sub-vertical down-thrusting (delamination) of the lithosphere at the margin, producing sharp vertical cold boundary down to the 400 km depth; (3) plume head flattening and migration towards the younger plate results in concurrent surface extension above the centre of the plume and in compression (pushing), down-thrusting and magmatic events at the cratonic margin (down-thrusting is also produced at the opposite border of the younger plate); these processes may result in continental growth at the "craton side"; (4) topographic signatures of PLI show basin-scale uplifts and subsidences preferentially located at cratonic margins. Negative Rayleigh-Taylor instabilities in the lithosphere above the plume head provide a mechanism for crustal delamination. Inferred consequences of PLI near intra-continental plate boundaries, such as faulting at cratonic edges and enhanced magmatic activity, could explain plume-related metallogenic crises, as suggested for West Africa and Australia.

Plume head –lithosphere interactions near intra-continental plate boundaries.

Evgene Burov[1], L. Guillou-Frottier[2], E. d'Acremont[1], L .Le Pourhiet[3], and S. Cloetingh[4]

[1]Laboratoire de Tectonique, Université Pierre & Marie Curie, Paris, France; evgenii.burov@lgs.jussieu.fr
[2]Service des Ressources Minérales, Bureau de Recherches Géologiques et Minières, Orléans, France, l.guillou-frottier@brgm.fr
[3]Geological and Planetary Sciences, California Institute of Technology, Pasadena,USA, laetitia@gps.caltech.edu
[4]Department of Earth Sciences, Vrije University, Amsterdam, Netherlands; cloeting@geo.vu.nl

Abstract

Plume-lithosphere interactions (PLI) have important consequences both for tectonic and mineralogical evolution of the lithosphere: for example, Archean metallogenic crises at the boundaries of the West African and Australian cratons coincide with postulated plume events. In continents, PLI are often located near boundaries between younger plates (e.g., orogenic) and older stable plates (e.g., cratons), which represent important geometrical, thermal and rheological barriers that interact with the emplacement of the plume head (e.g., Archean West Africa, East Africa, Pannonian – Carpathian system). The observable PLI signatures are conditioned by plume dynamics but also by lithosphere rheology and structure. We address the latter problem by considering a free-surface numerical model of PLI with two stratified elasto-viscous-plastic (EVP) lithospheric plates, one of which is older and thicker than another. The results show that: (1) plume head flattening is asymmetric, it is blocked from one side by the cold vertical boundary of the older plate, which leads to the mechanical decoupling of the crust from the mantle lithosphere, and to localized faulting at the cratonic margin; (2) the return flow from the plume head results in sub-vertical down-thrusting (delamination) of the lithosphere at the margin, producing sharp vertical cold boundary down to the 400 km depth; (3) plume head flattening and migration towards the younger plate results in concurrent surface extension above the centre of the plume and in compression (pushing), down-thrusting and magmatic events at the cratonic margin (down-thrusting is also produced at the opposite border of the younger plate); these processes may result in continental growth at the "craton side"; (4) topographic signatures of PLI show basin-scale uplifts and subsidences preferentially located at cratonic margins. Negative Rayleigh-Taylor instabilities in the lithosphere above the plume head provide a mechanism for crustal delamination. Inferred consequences of PLI near intra-continental plate boundaries, such as faulting at cratonic edges and enhanced magmatic activity, could explain plume-related metallogenic crises, as suggested for West Africa and Australia.

Key words: *plume-lithosphere interaction; cratons; metallogenic crises ; rheology*.

1. Introduction

Mantle plumes are regarded as focused mantle upwellings that originate from deep mantle sources (e.g., Campbell et al., 1989; Campbell and Griffiths, 1990; Olson, 1990). If the link with the source region is continuous, such upwellings are considered as mantle plumes *senso stricto*, otherwise they are referred as mantle "diapirs" *senso lato*. Yet, there is no difference in physical mechanisms driving "plumes" and "diapirs", and in nature it is difficult to discriminate between, continuous, multiple discontinuous or interrupted continuous mantle upwellings. For this reason, we call here "plumes" all focused plate-scale mantle upwellings. This is justified by the fact that, in this study, we focus only on the initial response of the lithosphere to plume head emplacement.

The possible consequences of plume-lithosphere interactions and even the existence of mantle plumes are topic of vivid discussions (e.g., Anderson, 1982; 1998; Farnetani et al., 1996; Ebinger and Sleep, 1998; Sleep, 1997, 2003a,b; Sleep et al., 2002; Sheth, 1999; Tackley, 2000; Foulger, 2002; Nyblade and Sleep, 2003, Ingle and Coffin, 2004). These discussions are not only fuelled by ambiguous observational evidence for the existence of mantle plumes but also – and at a large extent – by the discrepancies between the geological and geophysical observations and model-based predictions for consequences of plume-lithosphere interactions such as the expected large-scale (> 1000 km) dynamic topography, thermal, tomographic and gravity anomalies. Indeed, in their classical definition, mantle plumes should be associated with a large-scale domal uplift at surface and volcanic activity. However, these features are not always or unambiguously observed in the areas that present other signatures of plume activity, including such undisputable hot spots as Hawaii (e.g., Davies, 1988; 1992; Wessel and Keating, 1994). For example, the dynamic topography detected in the "Afar Triangle" – Red Sea zone differs from a large-scale

domal uplift, although there is little doubt in presence of large scale mantle anomaly below this area that bears tomographic (e.g. Pik et al., 2006) but also some geo-chemical signatures of a mantle plume (e.g., Moreira et al., 1996).

Despite of the difficulties of their detection, mantle plumes exist and have considerable impact on tectonic evolution of plates, because they can rapidly bring deep material to the surface, such as Fe+Mg rich magmas (e.g. Isley and Abbott, 1999; Ebinger and Sleep, 1998; Sleep et al., 2002; Sleep, 2003a,b; Nyblade and Sleep, 2003). The plumes may also trigger heating and melting of the lower crust and mantle lithosphere thus leading to crustal or mantle delamination (Smithies et al., 2003; Saleeby et al., 2003) and continental growth (Condie, 2002; McCullogh and Bennet, 1994). A number of advanced plume-lithosphere interaction models have considered various aspects of these interactions assuming self consistent starting conditions and treating complicated problems such as longevity of xenoliths at the base of the lithosphere and channeling of the plume material (e.g., Ebinger and Sleep, 1998; Sleep et al., 2002; Sleep, 2003a,b; Nyblade and Sleep, 2003). Recent tectonically-oriented models incorporate rheologically stratified lithosphere with a free-surface (d'Acremont et al., 2003; Burov and Guillou-Frottier, 2005; Guillou-Frottier et al., 2006). The models show that plumes can create particular small-scale topographic signatures such as the succession of uplift and subsidence phases. Finally, plumes may enable lithospheric faulting (d'Acremont et al., 2003; Burov and Guillou-Frottier, 2005) as well as crustal growth by accretion of juvenile magmas (Boher et al. 1992).

When a tectonically realistic formulation for the lithosphere is accounted for in models of plume-lithosphere interactions, the predicted surface deformation shows new intuitively unexpected features, and deeper lithosphere may become gravitationally unstable (Burov and Guillou-Frottier, 2005). Since variations in

lithospheric thickness and other heterogeneities are common in intracontinental settings (e.g., Artemieva and Mooney, 2002), a number of PLI-related geological issues cannot be tackled without considering lateral variations of lithosphere thickness. For example, lateral variations in thermal structure of the continental lithosphere, as underlined by Perry and Jaupart (2004); Mareschal and Jaupart (2004), should have strong implications for plume-lithosphere interactions near cratonic boundaries. To account for these phenomena we have conducted a series of new numerical models of PLI, in which we have included lateral heterogeneities associated with intra-continental plate boundaries. The models account for tectonically realistic lithospheric structure, free surface deformation and elastic-viscous-plastic (EVP) rheology of the lithosphere. The main goal of the experiments is to study plume – lithosphere interactions in tectonically realistic settings such as those that include intra-lithospheric blocks and cratonic borders. This study is also driven by the idea that surface signatures resulting from plume-continental lithosphere interaction near cratonic boundaries can explain a number of phenomena such as the concentration of magmatic activity at these boundaries or simultaneous extension-compression events. Predicted surface topography features are then used to interpret uplifts and subsidences in terms of mechanical coupling/uncoupling between different rheological layers within the lithosphere. In addition, heat and mass transfer at lithospheric depths, following the plume impact phase, is detailed and discussed in the framework of a number of well-known geological concepts such as continental growth or crustal delamination.

2. Plume-lithosphere interactions with a realistic formulation for the lithosphere

2.1 Plume physics, lithosphere layering and surface deformation

The physical side of the mantle plume concept includes upwelling of low density, high temperature and low viscosity mantle material separated from large-scale convective motions. When active, this upwelling is characterized by large geoid/topography ratio and can form a « superplume », i.e. a persisting diapir of a very large scale coming from D" boundary (e.g. Condie et al., 2000; Romanowicz and Gung, 2002), or smaller scale diapirs originating from different depths (Montelli et al., 2004; Courtillot et al., 2003; Ritter, 2005). When convection is not chaotic (high Raleigh and Reynolds numbers), the plume tail is connected to its "mushroom" head, but when more appropriate rheologies are considered (e.g., Davies, 1995; Trompert and Hansen, 1998) the plume can ascent in a chaotic regime with a high ascent rate.

The commonly predicted consequences of PH-CL (plume head – continental lithosphere) interactions are mainly derived from conventional fluid dynamics/viscous models of mantle convection (e.g., Cserepes et al., 2000; Farnetani et al., 1996; Nyblade and Sleep, 2003). The predictive power of these models for surface features is limited because they are not designed to adequately account for the mechanical response of the lithosphere. In typical convective models (e.g., Doin et al., 1997; Solomatov and Moresi, 2000), the lithosphere is considered as a thin viscous or quasi-viscous layer with undeformable surface. This assumption might be partly acceptable for oceanic plates, but the continental lithosphere cannot be regarded as a thin layer because its thickness (150-300 km) constitutes 50% – 90% of the thickness of the convective part of the upper mantle (350 – 500 km). The continental lithosphere cannot be also regarded as a single layer, because, in contrast to oceanic lithosphere, the continents are highly stratified. This stratification counts 2 to 4 layers: a 30-70 km

thick highly buoyant quartz-rich crust, which may be subdivided into 2-3 sub-layers of different rheology, and a 60 – 250 km thick, negatively or neutrally buoyant olivine-rich mantle layer. The crustal sub-layers include a brittle-elastic-ductile upper, middle and lower crust. The ductile and other mechanical properties of these layers may be highly contrasting. For example, the upper crust is mainly brittle while the lower crust is mainly ductile. Due to the presence of quartz-rich aggregates and increasing temperature with depth, the lower crust may have a viscosity as low as 10^{20} – 10^{21} Pa s below 20 km depth, at temperature of 250°C – 400°C (e.g., Kirby and Kronenberg, 1987). In the underlying mantle lithosphere, the ductile creep is activated at considerably higher temperatures (750 – 800°C). This infers the presence of a weak separation layer (lower or middle crust) between the strong upper or intermediate crust and mantle lithosphere (e.g., Watts and Burov, 2003; Burov and Watts, 2006). The weak layer between the strong upper crust and lithospheric mantle allows them to deform relatively independently (Figure 1, Burov and Guillou-Frottier, 2005). The ductile crust serves not only as a decoupling layer but also as a damping layer because the deformation at its bottom may not be directly transmitted to its surface, and vise-versa. Indeed, depending on the rheology and temperature distribution, the thickness of the weak lower crustal layer may reach 15-20 km, while the vertical undulations of its bottom due to the plume impact (= Moho boundary, top of the mantle lithosphere) are not expected to exceed 1.5 km (e.g., Ribe and Christensen, 1994). These small undulations can be accommodated, or absorbed, within the lowermost parts of the ductile crust without congruent surface deformation. However, they also should produce some indirect impact on the surface. This impact may result from lateral and vertical shear flow in the ductile crust cased by the plum-related uplift of the Moho boundary. This flow exerts basal shear at the base of the upper (strong) crust,

that may result in its thinning and in expession-compression instabilities. The related surface signatures would primarily depend on the mechanical properties of the crust and less on the characteristics of the plume itself. Similarly, plume head emplacement below the strong mantle lithosphere would not only result in its large scale upward deflection but also in its thinning, basal erosion and extensional-compressional instabilities. In all cases, the wavelength of plum-related vertical undulations of the lithospheric layers will be proportional to 5-10 thicknesses of their resistant cores (10 – 50 km, Burov and Diament, 1995). This evokes wavelengths of deformation on the order of 50-400 km, or up to 1000 km in case of very strong lithosphere. Most of these wavelengths are smaller than the wavelengths usually attributed to the plume-related dynamic topography (> 500-1000 km). The thermo-mechanical consequences of PLI for surface geodynamics and geology thus appear to be largely dependent on the structure and rheological properties the continental lithosphere (Burov and Guillou-Frottier, 2005).

The idea that in continents, mantle deformation due to plume head impingement produces only moderate or strongly modulated impact on surface deformation, was confirmed by recent numerical studies that take into account the stratified elasto-viscous-plastic lithosphere (**Figure 1,** Burov and Guillou-Frottier, 2005;). As mentioned above, conventional monolayer models of plume-lithosphere interaction predict only long - wavelength deformation (> 1000 km) with dynamic topography of 1 – 1.5 km (Ribe and Christensen, 1994). In these models, surface deformation is not computed *senso stricto* but is estimated from the assumption that vertical undulations of lithosphere-mantle boundary are directly translated to the surface. This assumption is questionable not only because the mantle undulations can be accommodated, or damped within the thick ductile lower crust, but also because the crust exhibits visco-

elastic properties that permit relaxation of plume-related stresses over geologically important periods of time (up to 10 Myr).

2.2 Previous results: the need for lateral heterogeneities

After exploring some of the possible consequences of plume-lithosphere interactions, Burov and Guillou-Frottier (2005) have suggested that the continental lithosphere serves as a frequency modulator of plume impact, as it transforms the large-scale deformation of mantle-lithosphere boundary (> 1000 km wavelength) into a short- and mid-wavelength deformation (50 – 500 km wavelength) observed at the surface. This deformation occurs at “tectonic scales” (i.e., same scales as sedimentary basins or orogens) and can be directly observed. When the structure and rheology of continental lithosphere is taken into account in plume-lithosphere models (Burov and Guillou-Frottier, 2005), quite complex behavior is predicted: small and middle-scale deformation attenuates large-scale topographic features, and a series of uplifts and subsidences form. Some of the predicted behaviors evoke those usually attributed to “passive” tectonic events.

The study by Burov and Guillou-Frottier (2005) has also shown that as the plume head locally erodes and thins the lithosphere, the buoyant crust may be mechanically decoupled from the mantle lithosphere, either above the center of the plume head or at its borders. At the borders, the edge of the laterally spreading plume head intrudes between the positively buoyant crust and heavier mantle. As a result, the lithospheric mantle is separated from the buoyant crust and is down-thrusted forming a “slab” that is driven down with the return flow in the plume head. The intrusion of the spreading plume head into the lithospheric mantle results in the compression above the borders of the plume, whereas the lithosphere above its center is extended.

The two main results briefly described above, i.e. the development of a complex surface topography and the possible occurrence of lithospheric instabilities, are expected to be seriously affected by lateral heterogeneities of the lithosphere (e.g. presence of a cratonic root). As it was shown by Burov and Guillou-Frottier (2005), wavelengths and amplitudes of surface topography are highly dependent on thickness of crust and mantle lithosphere. Moreover, the spreading of the plume head that follows the initial impact (see examples in Burov and Guillou-Frottier, 2005) should be seriously hampered or even stopped by deepening of the lithosphere-asthenosphere boundary. As already suggested by several studies, variations in lithosphere thickness (Artemieva and Mooney, 2002) may help to focus strain and rift localization (Pascal et al., 2002; Davis and Slack, 2002), or may enhance the plume-induced decompression melting rate (Manglik and Christensen, 1997; 2006). Consequently, a new series of experiments including the presence of a cratonic root is needed, especially because numerous plume-related events would have occurred near margins of cratonic blocks. In particular, continental flood basalts (e.g. Deccan, Parana), some of which were recently called "cratonic flood basalts" (Silver et al., 2006), would have been erupted after abrupt stress changes in the lithosphere. The Archean greenstone belts that contain komatiites have been linked to plumes. In addition, some carbonatites and kimberlites may originate from plumes that have stalled beneath thick lithosphere (Erns and Buchan, 2003). Abundance of banded iron formations at the Archean-Proterozoic boundary (e.g. Western Australia, Brazil and Canada) as well as similar locations for other mineralized provinces (e.g. the east African gemstone belt), suggest that some very particular dynamical processes occur between Archean cratons, their adjacent belts, and the underlying mantle. Margins of cratonic blocks, associated with transition from younger lithosphere to older lithosphere, are characterized by lateral

variations in thermo-rheological structure and plate thickness, which are reflected in variations of plate strength. In these transitional zones, plume head material and heat may be channeled below plate boundaries producing a number of important effects such as localized plate weakening and basal erosion (e.g., Monnereau et al., 1993; Davies, 1994: Molnar and Jones, 2004) including rifting, localized thermal and magmatic activity, attenuation or amplification of the material contrasts between the neighboring lithospheric blocks. In the present study, numerical modelling of plume head – continental lithosphere interaction in the presence of lithospheric boundaries of the cratonic blocks has been performed for a variety of thermo-mechanical structures of the lithosphere. Models and results are presented in the next section. We then discuss geological implications of these results.

3. Model and Experiments

3.1. Model setup

Our experiments are based on the models and techniques developed in the previous parametric studies by Burov and Guillou-Frottier (2005) and d'Acremont et al. (2003). These studies have modelled plume – continental lithosphere interactions for various visco-elastic-plastic lithospheric structures, plume head sizes and Rayleigh numbers. We use the same approach based on the numerical code Para(o)voz derived from FLAC algorithm (Cundall, 1989; Poliakov et al., 1993). This method allows for handling realistic rheologies and upper surface boundary conditions. To account for all possible modes of lithospheric deformation and for consistent account of pressure and of free upper surface, this method solves Newtonian equations of motion (second law) in Lagrangean framework instead of flow equations (Navier-

Stokes) in Eulerian framework commonly used in plume models. The algorithm explicitly takes into account elastic-brittle-ductile properties of the continental lithosphere, and handles strain localization, which permits to model formation of brittle and ductile faults and shear zones. The free upper surface boundary condition allows for adequate account of deformation of lithospheric layers. Due to the explicit nature of the code, the temperature, gravity and pressure dependent body forces are computed directly without necessity to introduce additional assumptions like those of the reference thermal gradient. The last versions of the code were described in detail in (Burov and Poliakov, 2001; Burov et al., 2001; 2003; Burov and Guillou-Frottier, 2005). Therefore, we reduce the description of the method to a summary provided in Appendixes A and B.

3.1.1. Model geometries

In the first preliminary set of experiments, the lithosphere is vertically stratified but laterally homogeneous. In the second, main set of experiments we consider two bordering lithospheric plates of contrasting age and thickness (see next sections).

Following previous plume models (e.g., Ribe and Christensen, 1994), we skip the initial stages of plume rise, as they are of minor importance for near-surface evolution. The initial mantle plume is located at the base of the model box, and has a diameter of 100-200 km. We chose a spherical shape for the initial plume because translating viscous bodies take spherical shape in laminar regime at important distance from the surface (Batchelor, 1967). However, since the model plume is deformable, the choice of its initial geometry is of minor importance. The vertical size of the model is 650 km (upper mantle), its horizontal size is 1800 km (**Figure 2a**).

3.1.2. Density and rheological structure

Each element of the numerical grid is assigned its specific material phase defined as a subset of physical parameters of the corresponding material: density, thermal and rheology parameters (**Tables 1 and 2**). Instead of using viscous rheology that is common for plume and convection models, we use elastic-viscous-plastic (EVP) rheology, which is more realistic for the lithospheric part of the model. The EVP rheology can be represented as a serial (Maxwell type) elastic, viscous (ductile) and plastic (brittle) body:

$$\varepsilon_{ij} = \varepsilon_{ij\,e} + \varepsilon_{ij\,v} + \varepsilon_{ij\,p} \quad (1)$$

where ε_{ij} stands for the components of strain tensor and subscripts refer to “elastic”, “viscous” and “plastic” contributions to the total strain (see Appendix for formulations of the elastic, viscous and brittle rheologies used). The equation (1) is solved in the incremental form. Each strain increment is computed according to its constitutive law, or “rheological term”: linear elastic, non-associated Mohr-Coulomb plastic or non-linear power law ductile creep (Appendix).

The deep mantle part of the model is effectively viscous since at temperatures > 1330°C the viscous/ductile term provides largest contribution to the strain increment. Two notions of the effective viscosity can be associated with the equation (1). The first notion relates to the “true” effective viscosity of the non-linear viscous term determined as:

$$\mu_{eff} = \tau^{II} / \partial\varepsilon^{II}_{v}/\partial t \quad (2)$$

where τ^{II} is the effective shear stress (second invariant), ε^{II}_{v} is the effective incremental viscous strain (second invariant). The second notion relates to the apparent viscosity determined as:

$$\mu_{a} = \tau^{II}/\partial(\varepsilon_e + \varepsilon_v + \varepsilon_p)^{II}/\partial t \quad (3)$$

The numerical code uses the "true" viscosity (eq. 2), but the apparent viscosity is also evaluated on the output, for comparison with pure viscous models.

We use conventional density and rheology structure for the mantle and lithosphere (Turcotte and Schubert, 2002, **Figure 2a,b**). All models include 40 km thick crust and four horizontal rheological layers (**Tables 1** and **2**; Kirby and Kronenberg, 1987; Carter and Tsenn, 1987): (1) a 20 km thick quartz-rich upper crust with density of 2700 kg/m^3; (2) a 20 km thick quartz-rich lower crust with density of 2900 kg/m^3 (in some experiments we used diabase lower crust with density of 2980 kg/m^3); (3) a 60 or 160 km thick olivine mantle lithosphere with density of 3330 kg/m^3; (4) deeper mantle with reference density of ρ_m = 3330 kg/m^3 below the lithosphere (Turcotte and Schubert, 2002). Although the cratonic mantle may be chemically different from normal lithosphere (depletion), the recent data show that this has much smaller effect on its density than it was previously thought (e.g., Poudjom et al., 2001). For this reason we use the same density for the mantle of young and old lithosphere. The density of the plume has the same dependence on pressure as the background, so the absolute values of the background density are not important. A uniform numerical grid provides vertical and horizontal resolution of 5 km/element (**Figure 2a**). The lithosphere has 30 to 50 elements in vertical cross-section, which provides 10-15 times better resolution than typical plume models (e.g. Ribe and Christensen, 1994).

3.1.3. Mechanical boundary conditions.

The mechanical boundary conditions are assigned at the four sides of the model **(Figure 2a)**. The surface is free. At the left and right sides, the horizontal velocity is u_x=0. At the bottom, hydrostatic pressure is applied. All other components of

stress, displacement or velocity are free (e.g., horizontal boundaries have vertical free slip condition, the bottom has a horizontal free slip condition etc).

3.1.4. Thermal boundary and initial conditions. Key thermal parameters.

Zero outflow is set as lateral thermal condition at both sides of the model. Fixed temperatures of 0°C and 2000°C are imposed as surface and bottom boundary conditions, respectively (Table 2). The initial thermal condition refers to application of initial background geotherm. This geotherm is constructed by joining continental geotherm with deep mantle (adiabatic) geotherm. The continental geotherms are age-dependent and computed from the half-space cooling model of Parsons and Sclater (1977) and Burov and Diament (1995).

The thermal and rheological structure of the older plate refers to a thick (200 km) craton with a nearly steady geotherm (Parsons and Sclatter, 1977) that corresponds to a thermotectonic age of 800 Ma. This age is smaller than the geological age of cratons. However, the thermal structure of continental lithosphere becomes steady already after 400 Myr (e.g., Burov and Diament, 1995; Burov, 2007). Thus there is no significant difference in the thermal structure of a 800 Ma and 2000 May old plate. For these reasons we call “cratons” all thermally stable plates older than 400-800 Ma.

The thermotectonic age of the younger lithospheric plate has been varied from very young, weak and hot (50 Ma and 100 Ma) to “normal” (150Ma and 200 Ma) lithosphere. The thermotectonic age of 150-200Ma is of special importance for geodynamic implications as it characterizes the thermo-rheological state of many

continental plates (e.g., Burov, 2007). For example, the Alpine lithosphere was thermally reset in Jurassic time.

The combined (lithosphere + mantle) initial geotherm (Figure 2b) becomes adiabatic (approx. 0.3°C/km, Sleep, 2003b) at depths below 1330°C; the temperature slowly increases from 1330°C to 1400°C at 400 km depth, to 2000°C at 650 km depth (e.g., Ribe & Christensen, 1994). Peculiar features of the initial geotherm are of minor importance as the thermal field is continuously updated during further computations (Appendix A).

The initial thermal model is validated by computing key stagnant parameters according to (Salomatov, 1995; Salomatov and Moresi, 1995; Nyblade and Sleep, 2003; Sleep, 2003b). For that, basal heat flow, q_m , is first roughly estimated from:

$$\delta \approx k_c(T_c\text{-}T_{moho})/q_m + k_m(T_{moho} - T_0)/q_s = k(T_c\text{-}T_{moho})/q_m + h_c, \qquad (4)$$

where δ is the thickness of the "stagnant lid" (strong lithosphere), q_m is the basal heat flux, q_c is the mean crustal heat flux, T_c is the temperature at the bottom of the lid, T_{moho} is the temperature at Moho depth (36 km). For q_m=15-20 mWt m^{-2}, δ = 200-250 km (craton). For q_m = 30 mWt m^{-2}, δ = 120-150 km (normal lithosphere). In the stagnant mantle lithosphere, the effective viscosity drops exponentially as the temperature increases with depth (Figure 2, Appendix). The viscosity becomes nearly constant in the convecting sub-lithosphere mantle as the temperature gradient becomes adiabatic. The depth Z_{rheo} to the zone of transition from fast viscosity drop (pre-dominant thermal conduction, lithosphere) to nearly constant viscosity (predominant thermal advection, mantle) defines the rheological thickness of the lithosphere. This zone is referred as rheology boundary layer. This layer separates strong lithosphere ("stagnant lid") from weak convective mantle and its thickness characterizes the mechanical stability of the "lid". For deep mantle rheology (Table 2),

the estimated characteristic temperature length scale for viscosity reduction in the rheology boundary layer is T_η =50-65K. This length-scale yields temperature change, $T_{rheo,}$ across the rheology boundary layer. In our model, $T_{rheo,}$ is on the order of 120-150K (Sleep, 2003a):

$$T_{rheo} \approx 2.4\ T_\eta \approx (T_c - T_{moho})/\theta \approx 1/A, \quad (5)$$

where θ is Frank-Kamenetskii parameter (Solomatov, 1995), $\theta \approx A\Delta T$ where A (~ 10^{-2}) is the activation parameter in Schubert et al. (2001, p.618) notation. The thickness of the rheological boundary layer, Z_{rheo} can be estimated as (Nyblade and Sleep, 2003): $Z_{rheo} \approx T_{rheo}\delta/T_c$ = 50 km. Consequently, the characteristic stress scale, $\tau_b \sim (Z_{rheo}\, g\, \rho_m\, \alpha\, T_{rheo}) \approx$ 5-7 MPa. Using the estimate for τ_b, we verify if the model craton would be stagnant in the absence of a plume. For the geotherms and rheology used (Figure 2b), the strength of the model craton is higher than τ_b down to the depth of 200-250 km. Depending on the age (50 to 200 Ma), the strength of the younger lithosphere is higher than τ_b down to the depth of 100 – 150 km (Figure 2b). For τ_b~5 – 7MPa and typical tectonic strain rates of 10^{-14} - $10^{-15}s^{-1}$, the effective mantle viscosity is on the order of 10^{20} - 10^{21} Pa s, which is a reasonable value for the sub-lithosphere mantle.

The horizontally variable lithospheric structure and “stagnant-lid” convection at the base of the lithosphere may modulate plume convection (Sleep, 2003a). The conventional Rayleigh number is thus not informative, and one needs a specific “plume” Rayleigh number or plume Stokes velocity to characterize the model (e.g., Burov and Guillou-Frottier, 2005). Nevertheless, our model is automatically self-consistent because the temperature field is updated at each time step and the buoyancy forces are re-adjusted according to the actual (and not reference) thermal distribution.

3.2. Results

The results of the experiments are shown in the **Figures 3 to 7**. We have started from the simplest scenario that considers a single continental plate impinged by a rising plume (**Figure 3**) and then introduced two plates of different age (**Figures 4, 5, 6**). In the following we describe in detail experiments with most representative 150 Ma continental plate bordering a near steady craton. The results of experiments with 50, 100 and 200 Ma plates are outlined in the summary of **Figure 7**.

3.2.1. Laterally homogeneous lithosphere (benchmark reference experiment).

Experiments with a single "normal" (150Ma geotherm) lithosphere (**Figure 3**) show that such lithosphere develops RT instabilities at its base, as a consequence of the plume impact (Cloetingh et al, 2004; d'Acremont et al., 2003; Burov and Guillou-Frottier, 2005). These instabilities are accelerated by the return flow at the borders of the plume head. The plume head arrives at sub-lithospheric depth 0.5 –1 Ma after its initialization (this time is compatible with the results of Burov and Guillou-Frottier, 2005). Plume head emplacement commences at about 2 Ma and achieves an apex at 5-6 Ma after. At this stage the plume destabilizes the colder (and consequently denser) mantle lithosphere in the areas adjacent to its borders. As the plume head arrives at the base of the lithospheric plate, it starts to flatten horizontally, which results in: (1) initial regional domal uplift of the surface (1000-1500m), (2) mechanical erosion of the lithosphere above the centre of the plume head, (3) differential mantle thinning, (4) forced delamination of the lithospheric mantle from the crust, and (5) down-thrusting of this mantle at the plume head borders. At 15 Ma this down-thrusting forms a negative mantle downwelling reaching 400-500 km depth. The lithosphere above the plume head undergoes thermal weakening and important differential thinning, which is

most prominent in the mantle part (**Figure 3**); the thickness of the resistant core of the mantle lithosphere is reduced by a factor of 3-5 already 10 Ma after plume initialization. As to the initial domal uplift, in less than 1-2 Myr it is replaced by a 300 km wide central basin surrounded by elevated flanks and two secondary basins. This subsidence occurs when the plume head touches the base of the lithosphere at 1 – 2 Ma. At 5 Ma the secondary basins move away as the plume head spreads laterally and the central basin continues to widen (600 km). At the same time, lithospheric mantle in the central zone is destabilized due to a negative RT instability and is sagged down inside the plume head, obviously because it is colder and thus denser than the plum material. At about 10 Ma since plume head emplacement, a series of new small basins/rifts and 500 m elevations form at surface. The undulations are spaced 200 – 400 km, while there is no more detectable remnants of the initial large-scale dome.

3.2.2. Young lithosphere and a craton, plume rising below the lithosphere-craton boundary.

The second set of experiments (**Figure 4**) explores the consequences of plume-lithosphere interaction below the transition between weaker and hotter “young” or “normal” lithosphere and an old cold thick “craton” lithosphere of 400-800 Ma age (analogous to the Eastern European plate). We vary the thermotectonic age of the younger lithosphere from 50 Ma to 200 Ma.

Experiments with 50, 100 and 150 and 200 Ma old lithosphere (Figures 4 and 7). In these experiments, sharp change in the vertical density and thermal structure at the boundary between cold craton and younger lithosphere leads to development of a marginal gravitational instability. Such instability may result either in

a drip-off of the border material or in smoothing of the border. In the beginning (frist 2Myr), the vertical border of the craton starts to collapse, that is, it gets smoothed due to the horizontal pressure gradient across the boundary between the lithospheres. Yet, when the laterally spreading plum head material reaches the cratonic boundary, it pushes aside and drags down the material of the craton boundary resulting in restoration and even in downward stretching of the initial vertical boundary between the younger and older lithosphere. The difference in the thermo-rheological structure between the two lithospheres eases preferential plume flattening under the younger hotter and weaker lithosphere. Horizontally spreading plume head material produces multiple instabilities in the overlying lithospheric mantle, in particular, drip-like down-sagging of this heavier mantle with some bits of the lower crust inside the plume head. At the border of the plume head, the mantle lithosphere delaminates from the positively buoyant part of the crust and starts to sink down. An asymmetric domal uplift of approximately 1500 m initially forms above the plume head. The amplitude of local shorter-wavelength deformations, for example above the plate borders, later reaches 2000-3000 m. Upwellings of hot material arriving from the flattening plume head erode mantle lithosphere and stall at Moho boundary. At this boundary, the upwellings are blocked by higher buoyancy of the continental crust (density of 2700 – 2900 kg/m^3). Large amounts of hot mantle plume material thus can be stocked below the Moho for an important period of time, and only a fraction of light magmas produced by partial melting of this material may be able to ascend to the surface through dikes or by pluton emplacement. In such contexts, the absence of magmatic events should not be interpreted as a decisive evidence for the absence of plume event. In this study, we do not model partial melting. However, it may be suggested that even if some melts/magmatic events will be observed at surface, they will not necessary have

unambiguous deep signatures as the hot sub-Moho reservoir also serves as heat source for crustal melting and thus may produce induce crustal melting.

The difference between very young (50Ma-100Ma) and older (colder and more resistant) normal lithosphere (150Ma and 200Ma, Figures 4,7) is that the domal surface uplift is rapidly replaced by series of smaller scale ups and downs. The other features basically resemble the case of young lithospheres except that hot material is less penetrative upwards but has a higher ability for horizontal flattening. In this case it also has a higher ability for producing gravity instabilities at the bottom of the overlying lithosphere (because of higher density contrast). In all cases, plume head spreads asymmetrically: it propagates to a much larger distance towards the external boundary of the normal lithosphere than towards the craton. The plume erodes a part of the normal lithosphere and provokes down-thrusting of the lithospheric mantle at the front of the laterally propagating plume head material.

3.2.3. Normal (younger) lithosphere and a craton, plume rising below the normal lithosphere.

Experiments with 50, 100 ,150 and 200 Ma old plate (Figures 5 and 7). In this set of experiments, the plume ascends below the normal lithosphere, 300 km away from the cratonic border (**Figure 5**). As in the previous experiments, the gravitational instability of the cratonic border ,is prevented by horizontal push from the laterally spreading plume head. Near the border, this spreading transforms in the localized downward return flow in the plume head. This flow drags the cratonic material down and forms a sharp vertical boundary between the plume and the craton. This cold high viscosity boundary prevents craton-ward propagation of the horizontally spreading plume head material, which is therefore channeled towards the weaker

normal lithosphere. This results in asymmetric flattening of the plume head and in preferential thinning of the normal lithosphere and in slab-like mantle down-thrusting at its borders. The down-thrusting of the borders of weaker and thinner lithosphere is less pronounced (200 km depth) than of the cratonic border, which material reaches the 350 km depth in 15 Myr (see temperature and effective viscosity field in **Figure 5b**). The total width of the normal lithosphere affected by thinning and weakening due to plume head flattening is about 1000 km, i.e. 5 times wider than the initial plume head diameter. The surface response to the plume head uprise shows moderate doming above the plume head almost compensated by subsidence due to regional extension and thinning of the lithosphere (right plot in **Figure 5a**).

Plume flattening is strongly asymmetric, with pronounced extension of the young lithosphere and with centre of spreading moving away from the craton-lithosphere boundary. The area above the plume head (extension) is surrounded by peripheral zone of compression and down-thrusting that form small compression belts. One of the striking features of the surface topography refers to the pronounced subsidence at the cratonic border (Figure 5a) caused by the subduction-like down-thrusting of the cratonic mantle. The resulting topography resembles that of the Pannonian basin – Carpathian transect (Cloetingh et al., 2004, see discussion below).

3.2.4 Normal (younger) lithosphere and a craton, plume rising below the craton.

Experiments with 50, 100, 150, 200 Ma old plate (Figures 6 and 7). In this set of experiments, the plume rises below the craton, 300 km away from its border (**Figure 6**). The hot plume head material arriving below the craton, erodes its central part and spreads horizontally to its borders (please note that on the right side of the

craton, the effect of this flow should be ignored due to the vicinity of the right wall of the model). The material arriving at the transition zone between the normal lithosphere heats up this zone considerably. The gravitationally unstable border of the craton then gets smoothed within 3Myr. The mantle of thermally-weakened normal lithosphere delaminates from the crust and is down-thrusted, together with the cratonic mantle, below the craton (see the material phase field in **Figure 6**). It may be suggested that the flow of the plum material to the cratonic borders may produce some volcanic activity focalized at the transition zone between the normal lithosphere and the craton. It is also noteworthy that surface topography of the craton is strongly affected by the spreading of the plume: the central region of the craton takes plateau-lake shapes whereas the borders are characterized by vertical undulations (Figure 7b). We later discuss that this topography profile resembles the Tanzanian craton.

The plume impact produces a similar effect for all ages of the “normal” plate (50 – 200Ma). The major difference concerns the surface amplitude and wavelength that tend to increase with the plate age. Zones of extension and thermal heating are first localized at the borders of the craton but then start to move progressively away inside the normal lithosphere. These zones are more localized than in the case of hot initial lithosphere and in nature may present narrow deep rift basins. Importantly, these basins are found far away from the centre of the plume head.

4. Discussion. Implications for interaction between the upper mantle and lithospheric processes

Results of the experiments fit first-order rheological and geophysical features of a number of known areas where plume-lithosphere interactions are suspected, such

as the present-day active Pannonian – Carpathian system, or cratonic areas such as West Africa, Tanzania, southwest Australia, or possible plume-induced delamination of the Columbia River Flood Basalt Province (Hales et al., 2005; V. Camp, *personal communication*, 2006). A number of key results for mantle and lithosphere dynamics are detailed below with geological implications.

4.1. **Lithospheric thinning, extension and compression. Predicted upper mantle structure and constraints from seismic tomography**

The thermal structure of the upper mantle created at 12-14 Ma **(Figure 4)** after the arrival of the mantle plume displays a number of common features with the tomographic images of cratonic margins.

For example, one of the most striking features of Carpathians dynamics is the formation and evolution of the Focsani Depression, a 13 km thick Miocene-Pliocene basin (e.g. , Cloetingh et al., 2004), situated in the vicinity of the Vrancea earthquake cluster (Figure 8a) expressed in a “cold” 300-400 km deep tomographic anomaly (e.g. Wortel and Spakman, 2000). Whether or not this represents the present position of a Beniof plane is disputed, mostly because the peculiar 85° dip of the downgoing lithospheric “slab” is situated almost in the front of the orogen. This has been so far explained as a late Miocene to Pliocene roll-back effect in the SE Carpathians, which could have culminated when the subducting slab tore (slab detachment sensu) along the trend of the orogenic arc. The latter is commonly thought to have induced a rebound in the northern, torn, parts of the slab, and subsidence of the lower plate in the bending area, where the slab still holds its integrity: this occurred simultaneously with a fast migration towards the foreland, leading to the opening of the thick foredeep (Focsani) basin. One can suggest, however, that the Miocene plume that has initiated extension in the Pannonian basin could also drive down-thrusting of the lithosphere

around its borders (Figure 8a), which can explain the simultaneously occurring extension and compression in the surrounding Carpathians. In this context, particularly striking are the model-predicted downwellings of the cold mantle to depths of 300-400 km that can be matched with those observed in the Pannonian-Carpathian system (Cloetingh et al., 2004, Figure 8a). Inspection of the model shown in **Figures 4, 5 or 7** shows the presence of cold sub-vertical cratonic lithosphere down to the depth of 300 km flanked by attenuated thinned stretched lithosphere with a dramatic thinning of its mantle component (e.g., see viscosity structure in Figure 5b at 16.1My). This abrupt vertical transition between the two types of lithosphere is strikingly similar to the pronounced near vertical contrast in seismic velocities in the Vrancea zone (Wortel and Spakman, 2000, Figure 8a). The predicted down-thrusting of the normal lithosphere at the left border of the model (Figure 4, snapshots 5.2 and 11.3 My or viscosity structure in Figure 5b, snapshots 11 and 16.1My) also resembles cold down-wellings below the Western border of the Pannonian basin observed from the seismic tomography (Figure 8a) Consequently, our experiments may provide a simple explanation to: (1) simultaneous extension in the middle of the basin and compression at its borders, (2) the occurrence of anomalous thinning of the mantle lithosphere below the Pannonian basin, and (3) the extreme low flexural rigidities recorded in this basin strikingly contrasting with the presence of the relatively strong lithosphere in the surrounding areas (e.g., Wortel and Spakman, 2000; Cloetingh et al., 2004).

In the Tanzanian craton area (**Figure 8b, top**), two vertical cross-sections of velocity anomalies published in (Weeraratne et al., 2003) clearly show near vertical cratonic edges (high velocity zones, extending down to 150 km depth), some of which (south-west and north-east borders) being surrounded by 100km-wide low velocity zones. On the opposite side, the south-west border of the craton does not show such

a vertical boundary and is not associated with a low velocity zone. The regional tomographic model of Sebai et al. (2006) supports the possibility of hot material such as a plume head beneath the Tanzanian craton, as does the two-plume scenario of Lin et al. (2005).

4.2. Lithospheric instabilities and crustal growth

Formation and growth of continental crust has been associated with various accretionary processes, including oceanic plateau or island arc accretion, back-arc basin or normal oceanic crust accretion (e.g., Kusky and Polat, 1999; Condie, 2002). The plume head – craton margin interaction may in fact provide another mechanism for crustal growth, by lateral spreading of lower crustal material. Indeed, the physical possibility for lower crustal convective instability has been confirmed by (Jull and Kelemen, 2001), who found that the conditions needed for development of Rayleigh-Taylor (RT) instabilities on the time scale of 10 Myr can be reached within continental plates underlain by a mantle plume. Recently, a lithospheric instability has been proposed as a plume-activated mechanism of formation of flood basalts and topographic signatures. In particular, Hales et al. (2005) have suggested that the flood basalts of the Columbia River are associated with mantle dynamics of the Yellowstone hotspot. Hales et al. (2005) interpret these basalts and the particular topographic signatures of the area in terms of interactions between the convective downwelling and detachment of a dense plutonic root. These authors suggest that convective instabilities might have been triggerred by propagating hot mantle material north along the Precambrian continental margin, where an increase in lithosphere thickness is suggested (Artemieva and Mooney, 2002). Plume-induced horizontal migration of

deep continental material towards cratons edges may thus represent another mechanism for lateral growth of continental blocks.

Numerical experiments of **Figures 4 and 5** have demonstrated the possibility for Rayleigh-Taylor instabilities to occur few million years after the plume arrival at the base of the lithosphere. Thermal weakening of the lithosphere by plume head involves two types of RT instabilities, that we call "drip-like" and "slab-like" instabilities. The drip-like downwellings (easily identifiable in thermal fields of **Figure 4 and Figure 5b**) are located above the plume head center, where heating is most efficient. These dynamic features have been suggested by several authors to explain convective removal of the deep crust (e.g. Saleeby et al., 2003). Due to subsequent arrival of hot upwelling material, mixing of lithospheric and asthenospheric material destroys drip-like instabilities in a few million years. The slab-like instabilities seem to develop more slowly and to last longer. **Figure 5b** (thermal and viscosity fields) illustrate such instabilities, having formed at both edges of plume head. Spreading of plume head towards young lithosphere would probably have a mixing effect, similarly to drip-like instabilities. On the opposite side, the near-craton slab-like instability is entrained by the return downward flow of the plume material, leading to a deep subsidence of lithospheric material, despite its high viscosity. These two kinds of lithospheric instabilities may trigger and enhance melting processes, since the lithospheric material is brought in contact with hot mantle, especially near cratonic margins where hot plume head stalls. As result, focusing of newly formed crust at cratonic margins may favor continental growth.

In West Africa, the major evolution of Birimian crust (~2.1 Ga) was suggested to be completed in less than 50 Ma (Boher et al., 1992), allowing these authors to suggest an enhanced plume activity close to Archean nuclei followed by collision

between oceanic plateaus and the Man Archean craton. Geochemical mixing between mantle and lithospheric material (as for the "slab-like" lithospheric instability) would also fit the geochronological and petrological constraints detailed in Abouchami et al. (1990). In Western Australia, a similar scenario with a mantle plume event at 2.0 Ga around cratonic areas, has also been suggested by Pirajno (2004).

4.3. Lithospheric faulting and near-craton ore deposits

Deep suture zones, identified in **Figures 4-5,** tend to localize at cratonic margins and are associated with highest thermo-mechanical contrasts. Combined with a high melting potential, these sutures may provide pathways for fluids and granitoids to migrate upwards and form ore deposits (Kusky and Polat, 1999). Anomalous concentration of metals in the lithosphere has been associated with large-scale geodynamic processes (e.g. Neubauer et al., 2005), and the role of deep lithospheric structures and discontinuities has been outlined by several authors (e.g. Kutina et al., 2003). In particular, the role of plume head is often evoked (Barley et al., 1998; Pirajno 2000) to account for pulses of magmatism between 2.8 and 2.6 Ga and associated mineralization, such as gold-rich granite-greenstone terrains in the Superior Province and Yilgarn craton (e.g. Groves and Barley, 1994).

According to Isley and Abbott (1999), mantle plume activity in Proterozoic and Archean times correlates strongly with the ages of banded iron formations (BIFs). Indeed, Fe-rich (tholeitic) magmas are mainly erupted during mantle plume events, and it appears that BIFs are spatially correlated with Archean cratons. Another possible example relating cratonic area, ore deposits and lithospheric discontinuities is the east African gemstone belt, including the Tanzanian Ruby belt (Le Goff et al., 2004), several hundred of kilometers long nearby the eastern branch of the East

African rift. Thermobarometric conditions for genesis of these gemstones would involve particular isothermal deepening of lower crust, as identified with the "slab-like" lithospheric instability. Relations between archean cratons, diamond deposits and kimberlite events have also been discussed by several authors, among which O'Neill et al. (2005) focus on abrupt changes in lithospheric thickness to explain coeval lithospheric discontinuities and enhanced melt production.

4.4. Surface behavior

Depending on the assumed plate rheology, models predict initial doming before the plume emplacement, and localized subsidence during the emplacement. The latter is associated with extension and lithospheric instability downing inside the plume head (< 2 Ma, first rifting phase, Burov and Guillou-Frottier, 2005). This phase is followed, after 3-5 Ma, by a second rifting phase, which is associated with plume head flattening and is marked by uplifts (~ 1000 m) on the sides of the basin. Plume head flattening provokes tensional instabilities in the lithosphere, which result in formation of series of narrow basins. At the end, the system of highs and lows of intra-basin topography may develop, with wavelengths between 300 and 500 km. It is noteworthy that such wavelengths and periodic surface undulations are often attributed to tectonically induced lithospheric instabilities (e.g., Smith, 1975). In case of a plume rising below the normal lithosphere or below the cratonic margin, there is an important subsidence on the side of the craton and strong topography elevation on the side of the normal lithosphere after 10-16 Myr. This type of behavior is strikingly similar to what is observed in a number of plume-lithosphere interaction zones such as Pannonian basin (e.g., Cloetingh et al., 2004, Figure 8a), where East-Carpathian “foredeep” resembles the subsidence predicted in the model (Figure 4 and 5a),

whereas the East Carpathians mountains are formed on the weak lithosphere, which refers to the predicted uplift on the side of the normal lithosphere.

In the presence of highly contrasting plate boundaries (normal lithosphere – craton), when the plume head has begun to spread, surface topography shows particular areas where elevation gradients are higher than elsewhere (**Figures 4, 5a, 6, 7b**). In other words, surface topography above the cratonic area shows little variation whereas cratonic borders are characterized by short-scale undulations. **Figure 8b** shows west-east topographic profiles across the Tanzanian craton area, where a "topographic plateau" surrounded by short-scale topographic undulations can be identified, from latitude -2°S to -6°S (see also Weeraratne et al., 2003). Model results are highly consistent with such signatures (**Figure 7b**). Clearly, as shown in **Figure 7a**,**7b**, plume edges have much more impact on surface topography than the plume head center, above which the lithospheric stresses relax within first 1-4 millions of years.

5. Discussion and conclusions

Lateral heterogeneities in the lithospheric structure have four major effects on plume-lithosphere interactions:

(1) Horizontal plume head flattening is blocked from one side by cold vertical boundary of the craton, leading to crust – mantle decoupling, stress and heat concentration and faulting at the cratonic margin; mantle lithosphere can be thrusted down at both sides of the plum head as a result of lateral spreading of the plume head material.

(2) Horizontal push exerted on the cratonic boundary by the spreading plume, and the return flow from the plume head, may result in delamination and near vertical

down-thrusting of the mantle lithosphere at the cratonic margin producing sharp subvertical “cold” boundaries going down to the depths of up to 300-400 km. This delamination resembles the delamination of the “rheological boundary layer” at the bottom of the lithosphere predicted by Nyblade and Sleep (2003) for a mono-layer lithosphere. However, in case of stratified rheology, the delamination is likely to occur at Moho boundary or within the lower crust. A large part of the mantle lithosphere, and some part of the lower crust can be delaminated from the buoyant part of the crust and trapped by the spreading plume head.

(3) The presence of a cratonic boundary promotes asymmetric plume head flattening towards the younger plate, followed by surface extension and lithospheric down-thrusting both at the cratonic margin and at the far end of the young plate. This creates a possibility that extension and compression occur simultaneously; same process would result in enhanced melting events at cratonic edges, and favor continental growth at the side of the craton.

(4) Topographic signatures of the plume-lithosphere interaction show basin-scale uplifts and subsidences due to the interplay between rheological stratification, visco-elastic relaxation and plume-induced mantle instabilities. These signatures have “typical tectonic” wavelengths (< 500 km) while long-wavelength deformation usually associated with plume impact is almost undetectable.

Rayleigh-Taylor instabilities that develop at the top and the sides of the plume head provide a mechanism for crustal delamination. Lateral flow of mantle lithosphere, from plume head to the base of the craton, suggests a new mechanism for crustal growth, where surface magmatism is not required. Lithospheric faulting at cratonic edges and enhanced magmatic activity could explain the apparent plume-related metallogenic crises, as suggested for West Africa and Australia. Plume–lithosphere

interactions can explain a number of other key phenomena such as the simultaneous occurrence of climax of extension of the young plates/segments and climax of compression in the surrounding belts. This scenario is consistent with differential mantle lithosphere thinning of the younger plate.

This study suggests that the plume impact may have complex consequences for surface evolution. In particular, absence of magmatic events should not be interpreted as evidence for the absence of plume events. If some melts/magmatic events are observed at the surface, they will not necessary have unambiguous deep geochemical signatures, as the hot source plume material stalls below Moho and forms a long-lasting (10 to 100 Myr) sub-Moho reservoir. This should induce strong crustal melting that may overprint deeper signatures since crustal melts are generated at much lower temperatures than mantle, and produce light low-viscous rapidly ascending magmas. In addition, drip-like down-sagging of the lithospheric mantle and metamorphic lower crustal material inside the plume head may contaminate the latter and thus alter the geochemical signature of plume-related magmas. However, this conclusion needs further investigation as we did not take into account methamorphic phase changes in the crust and partial melting.

Acknowledgements

We are greatly thankful to N. Sleep and the anonymous reviewer for detailed and highly constructive comments. We thank for the financial support of BRGM (Bureau des Recherches Geologiques et Minieres). This is a BRGM contribution 4572 . The code Para(o)voz v.9d originates from Paravoz v.3 by Poliakov and Podladchikov (Poliakov *et al*., 1993).

References

References

Abouchami, W., Boher, M., Michard, A., and Albarede, F., 1990. A major 2.1 Ga event of mafic magmatism in west Africa : an early stage of crustal accretion, J. Geophys. Res., **95**, 17605-17629.

Anderson, D.L., 1982. Hotspots, polar wander, Mesozoic convection and the geoid, Nature, **297**, 391-393.

Anderson, D.L., 1998. The scales of mantle convection, Tectonophysics, **284**, 1-17.

Artemieva, I.M., and Mooney, W.D., 2002. On the relations between cratonic lithosphere thickness, plate motions, and basal drag, Tectonophysics, **358**, 211-231.

Barley, M.E., Pickard, A.L., and Sylvester, P.J., 1997. Emplacement of a large igneous province as a possible cause of banded iron formation 2.45 billion years ago, Nature, **385**, 55-58.

Barley, M.E., Krapez, B., Groves, D.I., and Kerrich, R., 1998. The Late Archean bonanza : metallogenic and environmental consequences of ther interaction between mantle plumes, lithospheric tectonics and global cyclicity, Precamb. Res., **91**, 65-90.

Batchelor, G.K., 1967. An Introduction to Fluid Dynamics, Cambridge Univ. Press, 615pp.

Bauer, S.J., & Handin, J., 1983. Thermal expansion and cracking of three confined, water-saturated igneous rocks to 800°C, Rock Mech. Rock Eng., **16**, 181-198.

Bercovici, D., Ricard, Y., & Schubert, G., 2001. A two-phase model for compaction and damage 3. Applications to shear localization and plate boundary formation, J. Geophys. Res., **106**, 8925-8939.

Boher, M., Abouchami, W., Michard, A., Albarède, F., & Arndt, N. T., 1992. Crustal growth in west Africa at 2.1 Ga, J. Geophys. Res., **97**, 345-369.

Burov, E.B., & Poliakov, A.N.B., 2001. Erosion and rheology controls on synrift and postrift evolution: Verifying old and new ideas using a fully coupled numerical model, J. Geophys. Res., **106**, 16461-16481.

Burov, E., Jolivet, L., Le Pourhiet, L., & Poliakov, A.N.B., 2001. A thermomechanical model of exhumation of high pressure (HP) and ultra-high pressure (UHP) metamorphic rocks in alpine-type collision belts, Tectonophysics, **342**, 113-136.

Burov, E.B., & Diament, M., 1995. The effective elastic thickness (Te) of continental lithosphere: What does it really mean?, J. Geophys. Res., **100**, 3905-3927.

Burov, E.B., Jaupart, C., & L. Guillou-Frottier, L., 2003. Ascent and emplacement of magma reservoirs in brittle-ductile upper crust, J. Geophys. Res., **108**, 2177, doi:10.1029/2002JB001904

Burov, E.B., & L. Guillou-Frottier, 2005. The plume head – continental lithosphere interaction using a tectonically realistic formulation for the lithosphere, Geophy. J. Int., **161**, 469-490.

Burov, E., A.B. Watts, 2006. The long-term strength of continental lithosphere: "jelly-sandwich" or "crème-brûlé"?, GSA Today, **16**, 1, doi: 10.1130/1052-5173(2006)016<4:TLTSOC.

Burov, E.B., Plate rheology and mechanics, Ed.: G. Schubert, 2007, *Treatise on Geophysics, Volume 6 – Crust and Lithosphere Dynamics* (Volume Edt. A.B. Watts), AGU-Elsevier, in press.

Byerlee, J., 1978. Rock friction and earthquake prediction, Pure Appl. Geophys., **116**, 615-626.

Campbell, I.H., Griffiths, R.W., and Hill, R.I., 1989. Melting in an Archean mantle plume: Heads it's basalts, tails it's komatites, Nature, **339**, 697-699.

Campbell, I.H. abd Griffiths, R.W., 1990. Implications of mantle plume structure for the evolution of flood basalts, Earth Planet. Sci. Lett., **99**, 79-93.

Carter, N.L., and Tsenn, M.C., 1987. Flow properties of continental lithosphere, Tectonophysics, **36**, 27-63.

Cloetingh, S., Burov, E., Matenco L., Toussaint, G., and G. Bertotti, 2004. Thermo-mechanical constraints for the continental collision mode in the SE Carpathians (Romania), Earth Planet. Sci. Letters, **218**(1-2), pp. 57-76.

Condie, K.C., 2002. Continental growth during a 1.9-Ga superplume event, J. Geodyn., **34**, 249-264.

Condie, K.C., Des Marais, and Abbott, 2000. Geologic evidence for a mantle superplume event at 1.9 Ga, Geochem. Geophys. Geosyst., **1**, Paper number 2000GC000095.

Courtillot, V., Davaille, A., Besse, J., & Stock, J., 2003. Three distinct types of hotspots in the Earth's mantle, Earth Planet. Sci. Lett., **205**, 295-308.

Cserepes, L., Christensen, U.R., & Ribe, N.M., 2000. Geoid height versus topography for a plume model of the Hawaian swell, Earth Planet. Sci. Lett., **178**, 29-38.

Cundall, P.A., 1989. Numerical experiments on localization in frictional materials, Ing. Arch., **59**, 148-159.

d'Acremont, E., Leroy, S., & Burov, E.B., 2003. Numerical modelling of a mantle plume: the plume head-lithosphere interaction in the formation of an oceanic large igneous province, Earth Planet. Sci. Lett., **206**, 379-396.

Davies, G.F., 1988, Ocean bathymetry and mantle convection. 1. Large-scale flow and hotspots, J. Geophys. Res., **93**, 10467-10480.

Davies, G. F., 1992, Temporal variation of the Hawaiian plume flux, Earth Planet. Sci. Lett., **113**, 277-286.

Davies, G. F., 1994. Thermomechanical erosion of the lithosphere by mantle plumes, J. Geophys. Res., **99**, 15709-15722.

Davies, G.F., 1995. Penetration of plates and plumes through the mantle transition zone, Earth Planet. Sci. Lett., **133**, 507-516.

Davis, P.M., and Slack, P.D., 2002. The uppermost mantle beneath the Kenya dome and relation to melting, rifting and uplift in East Africa, Geophys. Res. Lett., **29**, doi: 10.1029/2001GL013676

Doin, M.-P., Fleitout, L., & Christensen, U., 1997. Mantle convection and stability of depleted and undepleted continental lithosphere, J. Geophys. Res., **102**, 2771-2787.

Ebinger, C. J., and N. H. Sleep, 1998. Cenozoic magmatism throughout East Africa resulting from impact of a single plume, Nature, **395**, 1788-791.

Ernst, R.E., and K.L. Buchan, Recognizing mantle plumes in the geological record, Annual Rev. of Earth and Planet. Sci., **31**, 469-523, 2003.

Farnetani, C.G., Richards, M.A., and Ghiorso, M.S., 1996. Petrological models of magma evolution and deep crustal structure beneath hotspots and flood basalt provinces, Earth Planet. Sci. Lett., **143**, p. 81-94.

Foulger, G., 2002. Plumes, or plate tectonic processes ?, Astr. Geophys., **43**, 619-623.

Gerbault, M., Poliakov, A.N.B., & Daignières, M., 1998. Prediction of faulting from the theories of elasticity and plasticity; what are the limits?, J. Struct. Geol., **20**, 301-320.

Goes, S., F. Cammarano, U. Hansen, 2004. Synthetic seismic signature of thermal mantle plumes, Earth Planet. Sci. Lett., **218**, 403-419.

Groves, D.I., and Barley, M.E., 1994, Archean mineralization, in: Archean Crustal Evolution, Condie, K.C. (ed.), Elsevier, Amsterdam, 528pp.

Guillou-Frottier, L., Burov, E., Nehlig, P., and R. Wyns, 2006, Deciphering plume-lithosphere interactions beneath Europe from topographic signatures, Global and Planetary Change, Spec. vol. on Topography of Europe, in press, 2006.

Hales, T.C., Abt, D.L., Humphreys, E.D., and Roering, J.J., 2005. A lithospheric instability origin for Columbia River flood basalts and Wallowa mountains uplift in northeast Oregon, Nature, **438**, 842-845.

Ingle, S., & Coffin, M.F., 2004. Impact origin for the greater Ontong Java plateau ?, Earth Planet. Sci. Lett., **218**, 123-134.

Isley, A.E., and Abbott, D.H., 1999. Plume-related mafic volcanism and the deposition of banded iron formation, J. Geophys. Res., **104**, 15,461-15,477.

Jull, M., and Kelemen, P.B., 2001, On the conditions for lower crustal convective instability, J. Geophys. Res., **106**, 6423-6446.

King, S.D., 2005. Archean cratons and mantle dynamics, Earth Planet. Sci. Lett., **234**, 1-14.

Kirby, S.H., and Kronenberg, A.K., 1987. Rheology of the lithosphere: selected topics, Rev. Geophys., **25**, 1219-1244.

Kohlstedt, D.L., Evans, B., & Mackwell, S.J., 1995. Strength of the lithosphere: constraints imposed by laboratory experiments, J. geophys. Res., **100**, 17587-17602.

Kukkonen, I.T., & Peltonen, P, 1999. Xenolith-controlled geotherm for the central Fennoscandian Shield: implications for lithosphere-astenosphere relations, Tectonophysics, **304**, 301-315.

Kusky, T.M., & Polat, A., 1999. Growth of granite-greenstone terranes at convergent margins, and stabilization of Archean cratons, Tectonophysics, **305**, 43-73.

Kutina, J., Pei, R., and Heyl, A.V., 2003, The role of deep lithospheric structure in the genesis and distribution of giant and supergiant concentrations of metals in the crust, Global tectonics & Metallogeny, **8**, 9-49.

Le Goff, E., Deschamps, Y., Muhongo, S., Cocherie, A., Milesi, J.P., Pinna, P., Msechu, M., and Mshihili, A., 2004. The Tanzanian "Ruby Belt":structural, petrological and geochronological constraints within the pan-African orogeny –

examples from the Morogoro and Mahenge districts, Colloquium of African Geology, CAG20, Orléans, France, 2-7 june 2004.

Lin, S-C., Kuo, B.Y., Chiao, L-Y, and van Keken, P.E., 2005. Thermal plume models and melt generation in East Africa : a dynamic modeling approach, Earth Planet. Sci. Lett., **237**, 175-192.

Manglik, A., & Christensen, U.R., 1997. Effect of mantle depletion buoyancy on ² flow and melting beneath a stationary plate, J. geophys Res., **102**, 5019-5028.

Manglik, A., & Christensen, U.R., 2006. Effect of lithospheric root on decompression melting in plume-lithosphere interaction models, Geophys. J. Int., **164**, 259-270.

Mareschal, J.-C., and Jaupart, C., 2004. Variations of surface heat flow and lithospheric thermal structure beneath the North American craton, Earth Planet. Sci. Lett., **223**, 65-77.

McCullogh, M.T., & Benett, V.C., 1994. Progresive growth of the Earth's continental crust and depleted mantle: geochemichal constraints, Geochim. Cosmochim. Acta, **58**, 4717-4738.

Molnar, P., and G.H. Jones, 2004. A test of laboratory based rheological parameters of olivine from an analysis of late Cenozoic convective removal of mantle lithosphere beneath the Sierra Nevada, California, USA, Geophys. J. Int., **156**, 555-564.

Monnereau, M., Rabinowicz, M., & Arquis, E., 1993. Mechanical erosion and reheating of the lithosphere: a numerical model for hotspot swells, J. Geophys. Res., **98**, 809-823.

Montelli, R., Nolet, G., Dahlen, F.A., Masters, G., Engdahl, E.R., & Hung, S.H., 2004. Finite-frequency tomography reveals a variety of plume in the mantle, Science, **303**, 338-343.

Moreira M., Valbracht P.J., Staudacher T. and Allègre C.J., 1996, Rare gas systematics in Red Sea ridge basalts, Geophys. Res. Lett., **23**, 182453-182456.

Morley, C.K., Wescott, W.A., Stone, D.M., Harper, R.M., Wigger, S.T., & Karanja, F.M., 1992. Tectonic evolution of the northern Kenyan rift, J. Geol. Soc. London, **149**, 333-348.

Neubauer, F., Lips, A., Kouzmanov, K., Lexa, J. & Ivascanu, P., 2005. Subduction, slab detachment and mineralization: the Neogene in the Apuseni mountains and Carpathians, Ore Geol. Rev., **27**, 13-44.

Nyblade, A. A., and N. H. Sleep, 2003, Long lasting epeirogenic uplift from mantle plumes and the origin of the Southern African Plateau, Geochem. Geophys. Geosystems, v. **4** (2003GC000573)

Olson, P., 1990. Hotspots, swells and mantle plumes, in Ryan M.P. (ed), Magma transport and storage, Wiley, Chichester, pp. 33-51.

O'Neill, C.J., Moresi, L., Jaques, A.L., 2005. Geodynamic controls on diamond deposits : implications for australian occurences, Tectonophysics, **404**, 217-236.

Parsons, B., & Sclater, J.G., 1977. An analysis of the variation of ocean floor bathymetry and heat flow with age, J. geophys. Res., **82**, 803-827.

Pascal, C., van Wijk, J.W., Cloetingh, S.AP.L., and Davies, G.R., 2002. Effect of lithosphere thickness heterogeneities in controlling rift localization : numerical modeling of the Oslo graben, Geophys. Res. Lett., **29**, 1355.

Perry, H.C., and Jaupart, C., 2004. Particular mantle dynamics induced by continental roots, Eos Trans. AGU, **85** (17), Jt. Assem. Suppl., Abstract T41C-04.

Pik, R., Marty, R., & Hilton, D.R., 2006. How many mantle plumes in Africa ? The geochemical point of view, Chem. Geol., **226**, 100-114.

Pirajno, F., 2000. Ore deposits and mantle plumes, Kluwer Acad., Dordrecht, Neth., 556 pp.

Pirajno, F., 2004. Oceanic plateau accretion onto the northwestern margin of the Yilgarn craton, western Australia : implications for a mantle plume event at ca. 2.0 Ga, J. Geodyn., **37**, 205-231.

Poliakov, A.N.B., Cundall, P., Podladchilov, Y., & Lyakhovsky, V., 1993. An explicit inertial method for the simulation of visco-elastic flow: an evaluation of elastic effects on diapiric flow in two- or three-layers models, in D.B. Stone & S.K. Runcorn (Eds), Flow and Creep in the Solar System: Observations, Modelling and Theory, Dynamic Modelling and Flow in the Earth and Planet Series, 175-195.

Poudjom Djomani, Y.H., O'Reilly, S.Y., Griffin, W.L. and Morgan, P., 2001. The density structure of subcontinental lithosphere: Constraints on delamination models, Earth Planet Sci. Lett., **184**, 605-621.

Ranalli, G., 1995. Rheology of the Earth, 2ndedn., Chapman and Hall, London, 413pp.

Ribe, N.M., and Christensen, U.R., 1994. Three-dimensional modeling of plume-lithosphere interaction, J. Geophys. Res. **99**, 669-682.

Ritter, J.R.R., 2005. Small-scale mantle plumes : imaging and geodynamic aspects, in Perspectives in Modern Geology, Wenzel, F. (ed), Lectures Notes in Earth Sciences, **105**, , Springer Verlag, Heidelberg, pp69-94.

Romanowicz, B., and Gung, Y.C., 2002. Superplumes from the core-mantle boundary to the base of the lithosphere, Science, **296**, 513-516.

Radulescu, F., Seismic models of the crustal structure in Romania, 1988. Rev. Roum. Géol. Géophys. Géogr. Sér. Géophys. **32**, 3-17.

Saleeby, J., Ducea, M., and Clemens-Knott, D., 2003. Production and loss of high-density batholitic root, southern Sierra Nevada, California, Tectonics, **22**, 1064 doi:10.1029/2002TC001374.

Schubert, G., Turcotte, D.L., and Olson, P., 2001. Mantle Convection in the Earth and Planets, Cambridge Univ. Press, 956pp.

Sebai, A., Stutzmann, E., Montagner, J.-P., Sicilia, D., and Beucler, E., 2006. Anisotropic structure of the African upper mantle from Rayleigh and Love wave tomography, Phys. Earth Planet. Int., **155**, 48-62.

Sheth, H.C., 1999. Flood basalts and large igneous provinces from deep mantle plumes: fact, fiction, and fallacy, Tectonophysics, **311**, 1-29.

Silver, P.G., Behn, M.D., Kelley, K., Schmitz, M., and Savage, B., 2006. Understanding cratonic flood basalts, Earth Planet. Sci Lett., **245**, 190-201.

Sleep, N., 1997. Lateral flow and ponding of starting plume material, J. geophys. Res.,**102**, 10001-10012.

Sleep, N. H., C. J. Ebinger, and J.-M. Kendall, 2002, Defection of mantle plume material by cratonic keels, in The Early Earth: Physical, Chemical and Biological Development, edited by C. M. R. Fowler, C.J. Ebinger and C.J. Hawkesworth, Geological Society London, Spec. Pub. **199**, 135-150.

Sleep, N., Survival of Archean cratonal lithosphere, 2003a. J. Geophys. Res., **108**, 2302, doi:10.1029/2001JB000169.

Sleep, N. H., 2003b. Geodynamic implications of xenolith geotherms, Geochem. Geophys. Geosystems, **4,** (2003GC000511).

Sleep, N. H., 2005. Evolution of continental lithosphere, Annual Rev. Earth Planet. Sci., **33**, 369-393.

Smith, R. B., 1975. Unified Theory of the Onset of Folding, Boudinage and Mullion Structure. Geol. Soc. Am. Bull., **88**, 1601-1609.

Smithies, R.H., Champion, D.C., and Cassidy, K.F., 2003. Formation of Earth's early Archean continental crust, Precamb. Res., **127**, 89-101.

Solomatov, V. S., 1995. Scaling of temperature- and stress-dependent viscosity convection, Phys. Fluids, **7**, 266–274.

Solomatov,V.S., & Moresi, L.N., 2000. Scaling of time-dependent stagnant lid convection; application to small-scale convection on Earth and other terrestrial planets, J. geophys. Res., **105**, 21795-21817.

Tackley, P.J., 2000. Mantle convection and plate tectonics; toward an integrated physical and chemical theory, Science, **288**, 2002-2007.

Trompert, R., & U. Hansen, 1998. Mantle convection simulations with rheologies that generate plate-like behaviour, Nature, **395**, 686-689.

Turcotte, D.L., & Schubert, G., 2002. Geodynamics, applications of Continuum Physics to Geological Problems, Second edition, Cambridge Univ. Press, 456 pp.

Watts, A.B., and E. Burov, 2003, Lithospheric strength and its relationship to the elastic and seismogenic layer thickness, Earth and Planet Sci. Letters, **213**, 113-131.

Weeraratne, D.S., Forsyth, D.W., Fischer, K.M., & Nyblade, A.A., 2003. Evidence for an upper mantle plume beneath the Tanzanian craton from Rayleigh wave tomography, J. Geophys. Res., **108**(B9), 2427, doi:10.1029/2002JB002273.

Weinberg, R.F., & Podladchikov, Y., 1994. Diapiric ascent of magmas through power law crust and mantle, J. geophys. Res., **99**, 9543-9559.

Wessel, P. and B. H. Keating, 1994, Temporal variations of flexural deformation in Hawaii, J. Geophys. Res., **99**, 2747-2756.

Wortel, M.J.R., & Spakman, W., 2000. Subduction and slab detachment in the Mediterranean-Carpathian region, Science, **290**, 1910-1917.

Figure captions

Figure 1 . Comparison of expected plate reaction to plume head impact in case of a single viscous layer (a) and a multilayer brittle-elastic-ductile plate model (b). In case of a tectonically realistic formulation for the continental lithosphere as in (b), surface topography shows periodic undulations at various wavelengths, and multiple zones of compression and extension are present. In this case, a part of lithosphere may be eroded and thrusted down at the edges of the plume head. Internal Rayleigh-Taylor instabilities (grey arrows) may also develop in the thermally weakened lithosphere above the plume head leading to drips-off of the lithosphere mantle and lower crust inside the plume head.

Figure 2a. The model setup (see description in the text). Left side of the model: younger continental lithosphere. Right side of the model: craton. Three initial positions of the plume were tested: plume centered below the plate boundary, 300 km away from the boundary below the younger lithosphere and 300 km away from the boundary below the craton. Color code: purple - crust, blue - mantle lithosphere, green – upper mantle, yellow- plume, orange – marker layer at the bottom that otherwise do not differ from the upper mantle.

Figure 2b. Initial lithospheric geotherms as a function of thermo-tectonic age (left), corresponding yield-stress envelops, computed for a constant strain rate of 10^{-15} s^{-1} (middle), and example of mantle-scale initial geotherm for craton (left). The lithosphere approaches thermal steady state starting from 400 Ma age, which also applies to its mechanical properties. In the present case, the upper crustal composition is dominated by quartz (granite), the lower crust is composed of diabase and the mantle is olivine controlled (Table 1).

Figure 3. Preliminary test with a single continental lithosphere of representative 150 Ma age and a 200 km-diameter plume. This experiment in based on the model from Burov and Guillou-Frottier (2005). Color code for the phase field: purple - crust, blue - mantle lithosphere, green – upper mantle, yellow - plume, orange – marker layer at the bottom. Note significant erosion of the mantle lithosphere, drip-like down-sagging of the lithospheric mantle, with some bits of the lower crust, above the middle of the

plume head, complex behavior of surface (periodic undulations / basins and uplifts). Surface topography (right) is obtained directly from the simulations. Circular diagrams show zones of plastic yielding (= faulting), following same graphical conventions as the Schmidt's diagrams for focal depth solutions used in seismology. Note that in nature drip-like instabilities may be enhanced by metamorphic phase changes in the lower crust that basically produce significantly denser material. The small secondary diapirs refer to the fact that we use a source layer at the bottom and fixed temperature boundary condition, instead of a localised infinite source region and fixed bottom heat flux as in some models. This assumption fits with recent tomography-based models (i.e. Goes et al., 2004) that suggest that plumes have thick tails comparable with their head size when they arrive to the upper-lower mantle boundary and then a smaller-headed plum with much thinner tail rises through the upper mantle.

Figure 4. Experiment with two plates (younger 150 Ma old lithosphere and 800 Ma old craton); plume head is located in the centre, below the plate boundary. Same color code as in Figure 3. Note significant erosion of the mantle lithosphere, "verticalization" of the cratonic boundary, multiple down-sagging of the lithospheric mantle above the middle of the plume head with hot material arriving at Moho depth, asymmetric flattening of the plume head towards the younger lithosphere, down-thrusting of the mantle lithosphere at both sides of the plume, and asymmetric doming at surface.

Figure 5a. Experiment like in Figure 4 but with plume head located below the younger lithosphere, 300 km away from intra-plate boundary. Note significant erosion of the mantle lithosphere, "verticalization" of the cratonic boundary, moderate extension and multiple down-sagging above the middle of the plume head with hot material arriving at Moho depth, asymmetric flattening of the plume head towards the younger lithosphere, down-thrusting of the mantle lithosphere at both sides of the plume, asymmetric doming at surface and multi-scale undulations.

Figure 5b. The effective viscosity (ratio of stress to strain rate for all, brittle, elastic and ductile domains) and temperature for the experiment shown in Figure 5a. Note down-thrusting of the mantle lithosphere at both sides of the plume, drip-like down-sagging above the middle of the plume head. Strong cratonic mantle delaminates from the crust and is "subducts" down the depth of 300 km ("slab-like" instability, in green in the temperature field). The mantle of younger lithosphere "subducts" to 200 km depth.

Figure 6. Experiment like in Figure 4 but with plume head located below the craton, 300 km away from plate boundary. Same color code as in Figure 3 Note significant erosion of the cratonic mantle lithosphere, asymmetric flattening of the plume head and down-thrusting “subduction” of the younger and cratonic mantle lithospheres below the craton, and permanence of a topographic "plateau" above the craton. The effect of plume head spreading on the right side of the craton should be ignored due to the vicinity of the boundary of the model.

Figure 7a. Comparison of mature stages (7.5 Myr since initialization) of experiments for different initial thermal ages (50, 100, 150, 200Ma) of the younger lithosphere (thermal field). Left column: plume rising below the younger plate; Middle – plume rising below the cratonic boundary; Right – plume rising below the craton. In all cases, the presence of intraplate boundary results in asymmetric plume spreading towards the younger lithosphere and in down-thrusting of the mantle lithosphere at plume borders.

Figure 7b. Comparison of developed stages of experiments for different initial thermal ages (topography). Left column: plume rising below the younger lithosphere; Middle – plume rising below the intraplate boundary; Right – plume rising below the craton. In all cases, the presence of intraplate boundary results in asymmetric surface features and in small scale (100 – 250 km) undulations superimposed onto larger scale features.

Figure 8a. Top: Crustal-scale cross-sections across the East Carpathians (modified after Radulescu (1988) and Cloetingh et al., (2004)). Red lines represent the northern crosssection in the area affected by the collision with the East European/Scythian rigid block. Blue lines represent the southern crosssection in the bend area in£uenced by the collision with highly buoyant Moesian block. Red dots represent earthquake projection into the southern section trace. Bottom: Seismic tomography (after Wortel and Spakman, 2000) across the bend zone of the East Carpathians in the MB domain.

Blue and red: positive and negative P-wave anomalies corresponding to the presence of cold and hot mantle in the area, respectively. Open circles give the location of Vrancea earthquakes.

Figure 8b. Topographic profiles across the Tanzanian craton area, where a "topographic plateau" surrounded by short-scale topographic undulations can be identified, from latitude -2°S to -6°S. Bottom: comparison with topographic signature generated by the models (Figure 7b). As shown in Figure 7a and 7b, in case of a plume ascending below a lithospheric plate of limited size, plume edges may have more impact on surface topography than the plume head center.

Table 1. Notations and physical values common for all experiments (Turcotte & Schubert, 2002; Schubert et al., 2001)

Parameter	Values and units	Definition
σ, τ	Pa, MPa	stress
P	Pa, MPa	pressure
$\mathbf{u}$	m s^{-1}, mm y^{-1}	velocity vector
μ	10^{19}-10^{25} Pa s	effective viscosity
$\dot{\varepsilon}$	s^{-1}	strain rate
T	°C	temperature
h_c	40 km	Moho depth
h_l	100 - 200 km	Thickness of lithosphere
D	100 - 200 km	plume diameter
ρ_l	3330 kg m^{-3}	Density of mantle lithosphere
ρ_m	3400 kg m^{-3}	reference mantle density (at 200 km depth)
ρ_p	$\rho_m + \Delta\rho_{ch} + \alpha\rho_m\Delta T$	plume density

$\Delta\rho_{ch}$	0-25 kg m^{-3}	Chemical density contrast
g	9.8 m s^{-2}	acceleration due to gravity
C_p	10^3 J kg^{-1} °C^{-1}	specific heat
ΔT	250°C	initial temperature contrast plume - background
α	3×10^{-5} °C^{-1}	thermal expansivity

Table 2. Specific rheology and related thermal parameters. Compilation by Burov *et al*. (2001). ρ is density; Q, n, A are material-dependent parameters of ductile flow laws (Kirby and Kronenberg, 1987; Kohlstedt et al., 1995). Other parameters from Turcotte and Schubert (2002).

Parameter	Value
All rocks	
λ , G Lamé elastic constants ($\lambda = G$)	30 GPa
ϕ friction angle (Mohr-Coulomb criterion)	30°
C_0 cohesion (Mohr-Coulomb criterion)	20 MPa
Specific properties of the crust (quartz dominated)	
ρ (upper crust)	2700 kg m^{-3}
ρ (lower crust)	2900 kg m^{-3}
n	2.4
A	6.7×10^{-6} $MPa^{-n} \cdot s^{-1}$
Q	1.56×10^{5} $kJ \cdot mol^{-1}$
Specific properties of strong lower crust (diabase)	
ρ	2980 kg m^{-3}
n	3.4
A	2×10^{-4} $MPa^{-n} \cdot s^{-1}$
Q	2.6×10^{5} $kJ \cdot mol^{-1}$
Specific mantle properties (olivine)	
ρ (lithosphere)	3330 kg m^{-3}
n	3
A	1×10^{4} $MPa^{-n} \cdot s^{-1}$
Q	5.2×10^{5} $kJ \cdot mol^{-1}$
Thermal model	
Surface temperature, T_0 (fixed)	0°C
Characteristic temperature at the bottom of the mechanical lithosphere	750°-1000°C

Characteristic temperature length scale for viscosity drop (Sleep, 2003b), T_η	50-60°C
Characteristic temperature change in rheological boundary layer, in Sleep (2003b) notation, T_{rheo}	~150°C
Initial base of thermal lithosphere, in Sleep (2003b) notation, T_c	1330°C
Temperature at 660 km depth (fixed), T_1	2000°C
Thermal conductivity of crust, k	2.5 Wm^{-1} °C^{-1}
Thermal conductivity of mantle, k	3.5 Wm^{-1} °C^{-1}
Thermal diffusivity of mantle, χ	10^{-6} $m^2.s^{-1}$
Thermal expansion, α	3×10^{-5} K^{-1}
Surface radiogenic heat production, H_s	9.5×10^{-10} W kg^{-1}
Radiogenic heat production decay depth, h_r	10 km
Thermotectonic age of the lithosphere, a	50-200Myr and 800 Myr (craton)

Appendix. Numerical model.

Basic equations. The Para(o)voz (previously Paravoz) is “2.5 D” FLAC-like code (Cundall, 1989). The term “2.5D” refers to the fact that strain/stress relations are solved in 3D formulation but the model geometry is cylindrical 2D (out-of plane boundary conditions for stress are set for plain stress)). The code has a mixed finite-difference/finite element numerical scheme, in which the coordinate frame is Cartesian 2D, but stress/strain relations are computed in 3D formulation. The Lagrangian mesh of Para(o)voz is composed of quadrilateral elements subdivided onto 2 couples of triangular sub-elements with tri-linear shape functions. Para(o)voz is a large strain fully explicit time-marching algorithm. It locally solves full Newtonian equations of motion in continuum mechanics approximation:

$$\langle \rho \dot{\mathbf{u}} \rangle - div\boldsymbol{\sigma} - \rho \mathbf{g} = 0 \qquad \text{(A1)}$$

coupled with constitutive equations:

$$\frac{D\sigma}{Dt} = F(\sigma, \varepsilon, \nabla \mathbf{u}, ...T...) \qquad \text{(A2)}$$

and with the equations of heat transfer:

$$\rho C_p \partial T/\partial t + \mathbf{u}\nabla T - k\, div(\nabla T) - H_r = 0$$

$$\rho = \rho_0(1-\alpha T) \qquad \text{(A3)}$$

Here $\mathbf{u}$, $\boldsymbol{\sigma}$, $\boldsymbol{g}$, k are the respective terms for velocity, stress, acceleration due to body forces and thermal conductivity. The triangular brackets in (A1) specify conditional use of the related term (in quasi-static mode inertial terms are dumped using inertial mass scaling (Cundall, 1989). The terms t, ρ, C_p, T and H_r designate respectively time, density, specific heat, temperature and internal heat production. The terms $\partial/\partial t$, $D\sigma/Dt$, F are a time derivative, an objective Jaumann time derivative of stress and a functional, respectively. In the Lagrangian method, incremental displacements are added to the grid coordinates allowing the mesh to move and deform with material. This enables solution of large-strain problems locally using small-strain formulation: on each time step the solution is obtained in local coordinates, which are then updated in large strain mode.

Solution of (A1) provides velocities at mesh points; these velocities are used for computation of element strains and of heat advection $\boldsymbol{u}\nabla T$. The strains are used in (A2) to calculate element stresses and forces; the forces are then used to compute velocities for the next time step. Due to the explicit approach, there are no convergence issues in case of non-linear rheologies. The algorithm automatically checks and adopts the internal time step using Courant's criterion for propagation of information, which warrants stable solution.

Explicit EVP rheology. We use serial (Maxwell type) body (eq. 1), in which total strain increment in each numeric element is defined by a sum of elastic, viscous and brittle strain increments. In contrast to fluid dynamic approaches, where non-viscous rheological terms are not implemented directly but simulated using pseudo-plastic and pseudo-elastic viscous terms (e.g. Bercovici et al., 2001; Solomatov and Moresi, 2000), our method explicitly treats all rheological terms. The parameters of elastic-ductile-plastic rheology laws for crust and mantle come from rock mechanics data (Tables 1 and 2; Kirby and Kronenberg, 1987; Kohlstedt et al., 1995).

Plastic (brittle) behavior. The brittle behavior of rocks is described by Byerlee's law (Byerlee, 1978; Ranalli, 1995), which corresponds to Mohr-Coulomb material with friction angle $\phi = 30°$, small dilatation angle (5°) and cohesion $|C_0| < 20$ MPa (e.g., Gerbault *et al*., 1998):

$$|\tau| = C_0 - \sigma_n \tan\phi \qquad \text{(A4)}$$

where σ_n is normal stress $\sigma_n = \frac{1}{3}\sigma_I + \sigma_{II}^{dev} \sin\phi$, $\frac{1}{3}\sigma_I = P$ is the effective pressure, σ_{II}^{dev} is the second invariant of deviatoric stress, or effective shear stress. The condition of transition to brittle deformation (function of rupture f) reads as: $f = \sigma_{II}^{dev} + P \sin\phi - C_0 \cos\phi = 0$ and $\partial f/\partial t = 0$. In terms of principal stresses, the equivalent of the yield criterion (5) reads as:

$$\sigma_1 - \sigma_3 = -\sin\phi\,(\sigma_1 + \sigma_3 - 2C_0/\tan\phi) \qquad \text{(A5)T}$$

Elastic behavior. The elastic behavior is described by linear Hooke's law:

$$\sigma_{ij} = \lambda\varepsilon_{ii}\delta_{ij} + 2G\varepsilon_{ij} \qquad \text{(A6)}$$

where λ and G are Lame's constants. Repeating indexes mean summation and δ is Kronecker's operator.

Viscous (ductile) behavior. Mantle convection and a part of lithospheric deformation is controlled by thermally activated creep (Ranalli, 1995; Kirby and

Kronenberg, 1987). Within deep lithosphere and underlying mantle regions, creeping flow is non-Newtonian since the effective viscosity can vary within 10 orders of magnitude as a function of differential stress:

$$e^{d}_{II} = A\,(\sigma_1 - \sigma_3)^{n} \exp(-Q\,R^{-1}T^{-1}) \qquad \text{(A7)}$$

Where $e^{d}_{II} = \dot{\varepsilon} = (\mathrm{Inv}_{II}(e_{ij}))^{1/2}$ is effective shear strain rate, A is material constant, n is power law exponent , Q is activation enthalpy, R is Boltzman's gaz constant, and T is temperature in K, σ_1 and σ_3 are the principal stresses. The effective viscosity μ_{eff} for this law is defined as:

$$\tau_{ij} \equiv \mu_{eff}\, e^{d}_{II}$$

which yields:

$$\mu_{eff} = e^{d}_{II}{}^{(1-n)/n}\, A^{-1/n} \exp(Q\,(nRT)^{-1}) \qquad \text{(A8)}$$

For non-uniaxial deformation, the law (A8) is converted to a triaxial form, using invariant of strain rate and geometrical proportionality factors:

$$\mu_{eff} = e^{d}_{II}{}^{(1-n)/n}\, (A^{*})^{-1/n} \exp(Q\,(nRT)^{-1})$$
$$\text{where } A^{*} = \tfrac{1}{2}A \cdot 3^{(n+1)/2} \qquad \text{(A9)}$$

parameters A, n, Q are experimentally determined material constants (Table 2). Using olivine parameters (Table 2), one can verify that the predicted effective viscosity at the base of the lithosphere is $10^{19} - 5 \times 10^{19}$ Pa s matching the post-glacial rebound data (Turcotte and Schubert, 2002). In the depth interval of 200 km - 0 km the effective viscosity exponentially grows from 10^{19} to 10^{25} - 10^{27} Pa s with decreasing temperature. Within the adiabatic temperature interval below 200 km depth, the viscosity slowly increases from $10^{19} - 10^{21}$ Pa s (e.g., Turcotte and Schubert, 2002). Weinberg and Podladchikov (1994) have also shown that the effective viscosity in close vicinity of an ascending diapir is influenced by local strain rate field and partly by heat exchanges between the diapir and surrounding rock. When such a diapir translates to the surface, the environment above and in the vicinity of the plum head is weakened, which eases its ascent (self-lubrification). .

Figure 1
Click here to download high resolution image

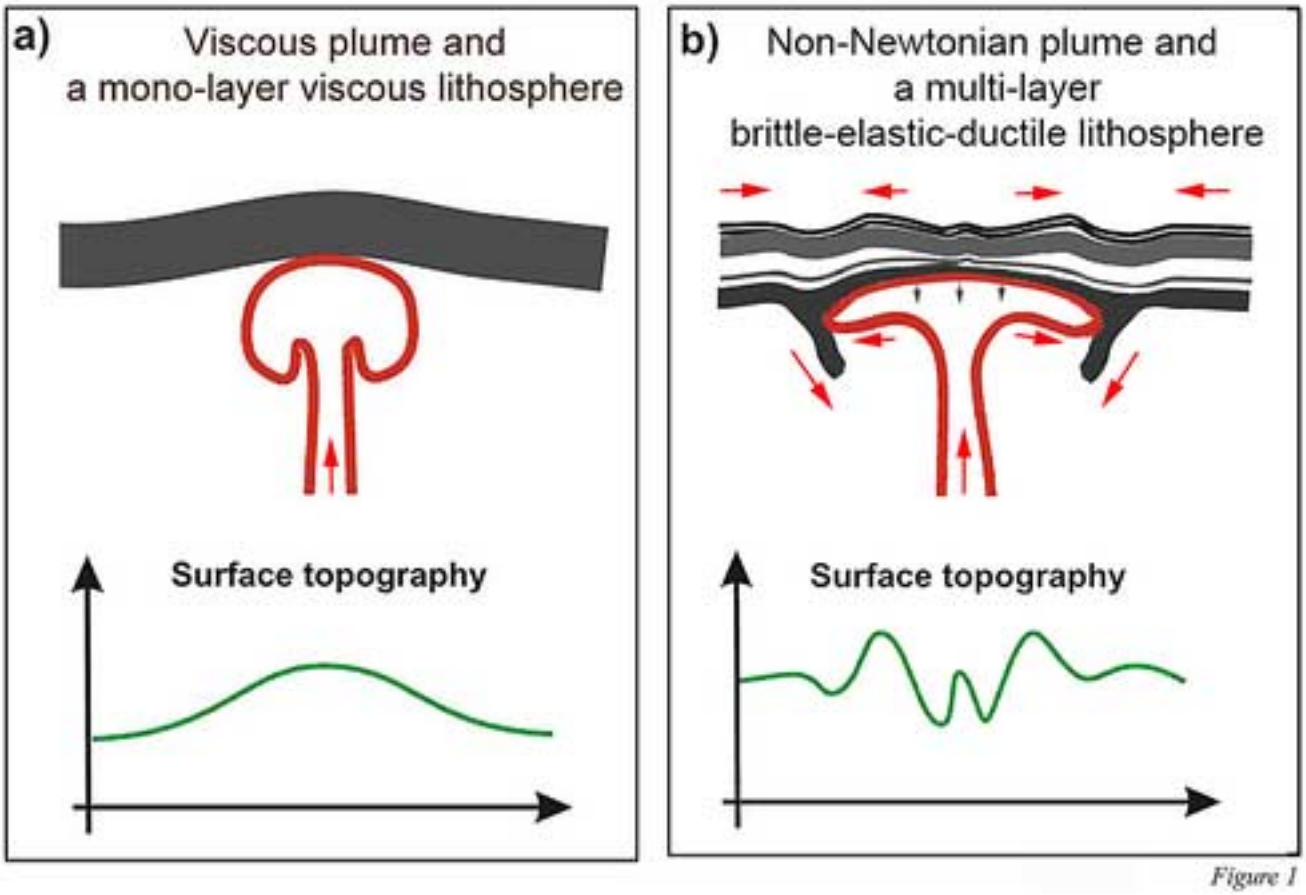

Figure 1

Figure 2a
Click here to download high resolution image

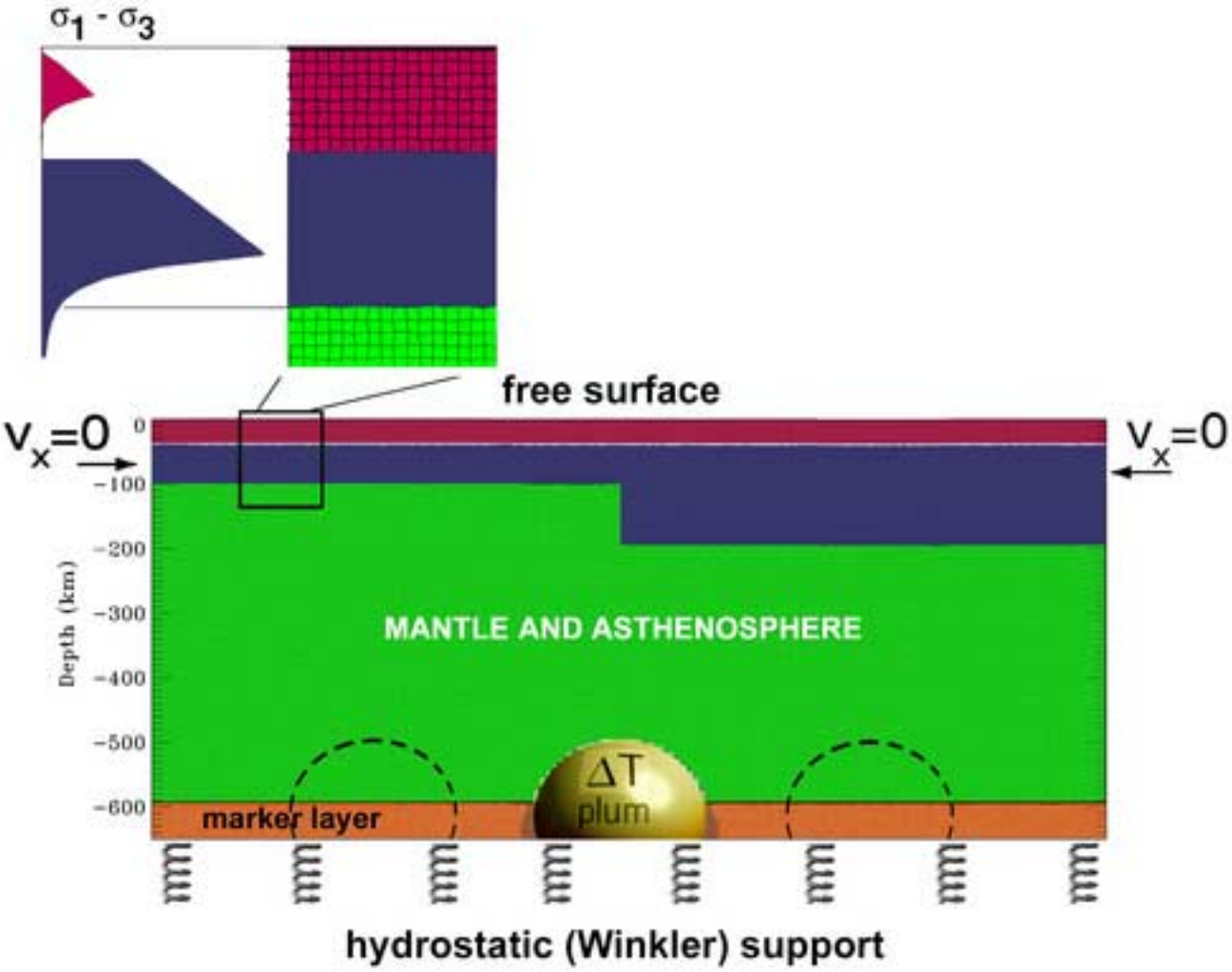

Figure 2a

Figure 2b

Click here to download high resolution image

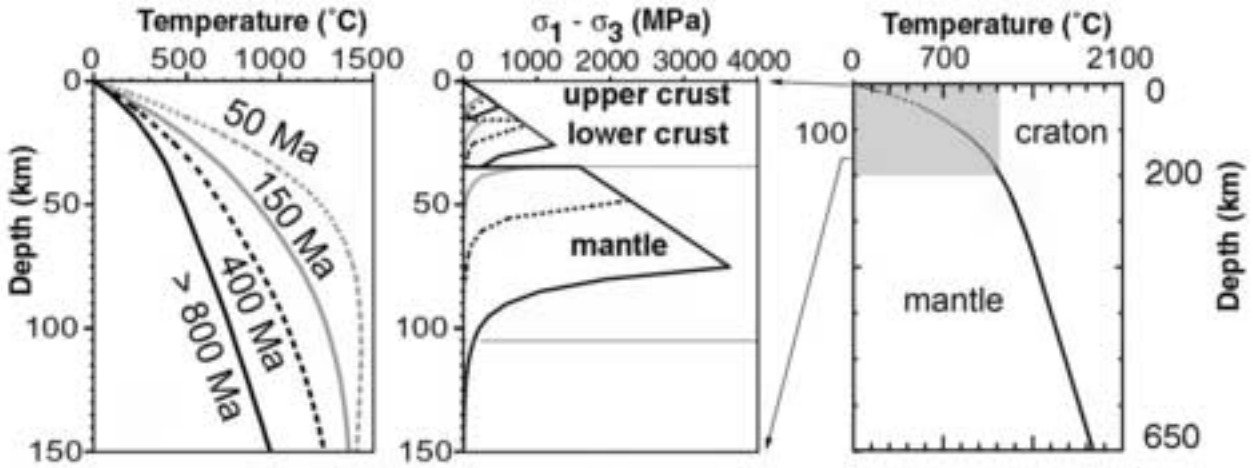

Figure 3

Click here to download high resolution image

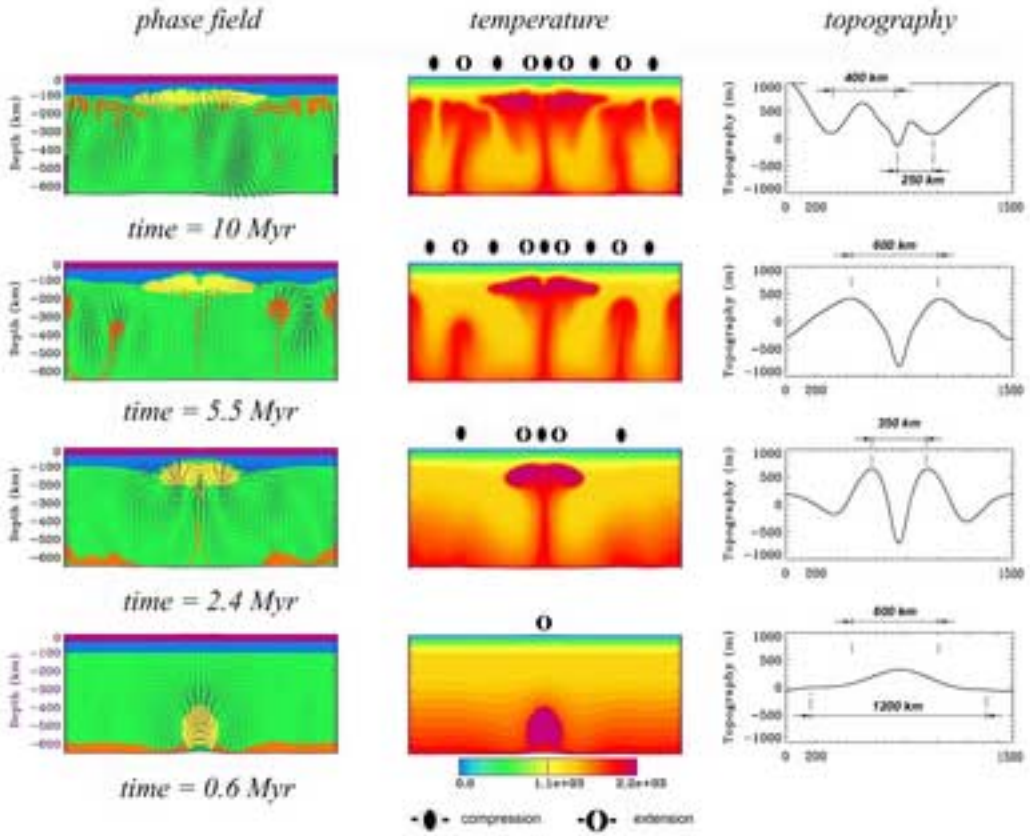

Figure 3

Figure 4
Click here to download high resolution image

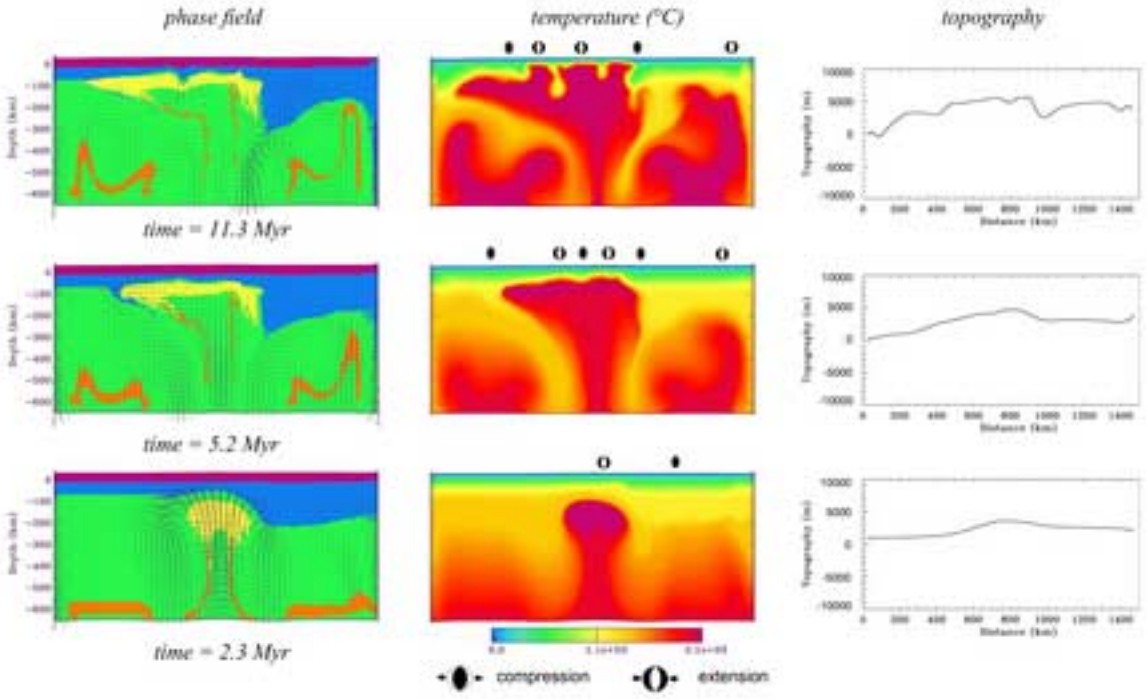

Figure 4

Figure 5a
Click here to download high resolution image

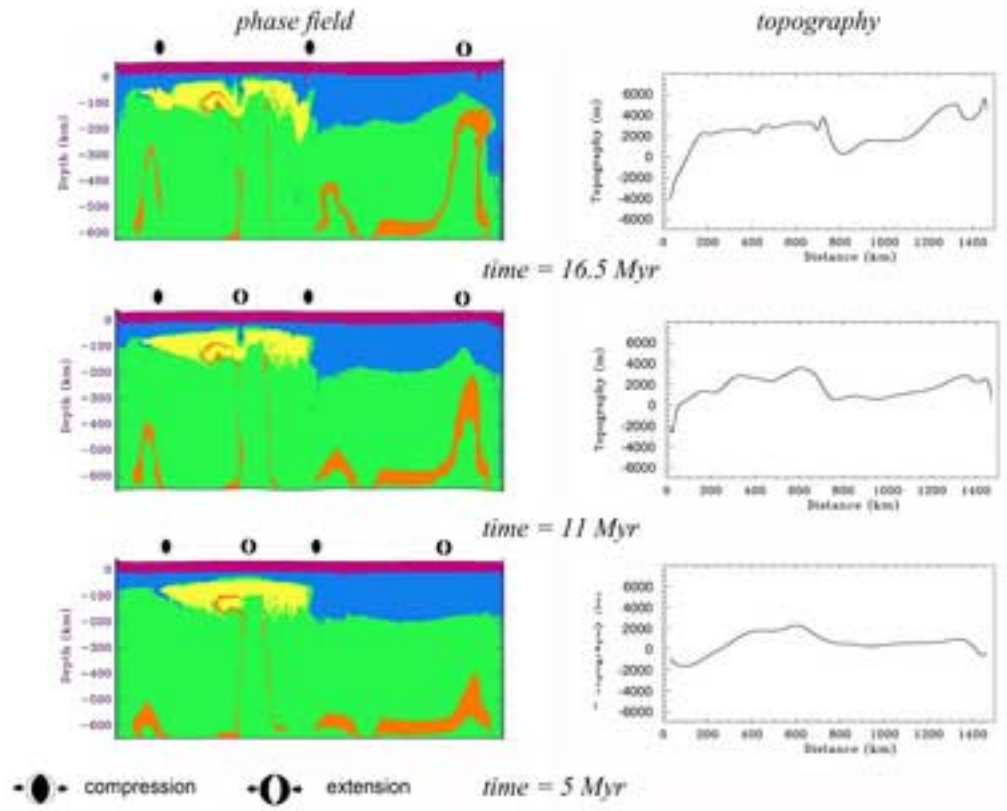

Figure 5a

Figure 5b
Click here to download high resolution image

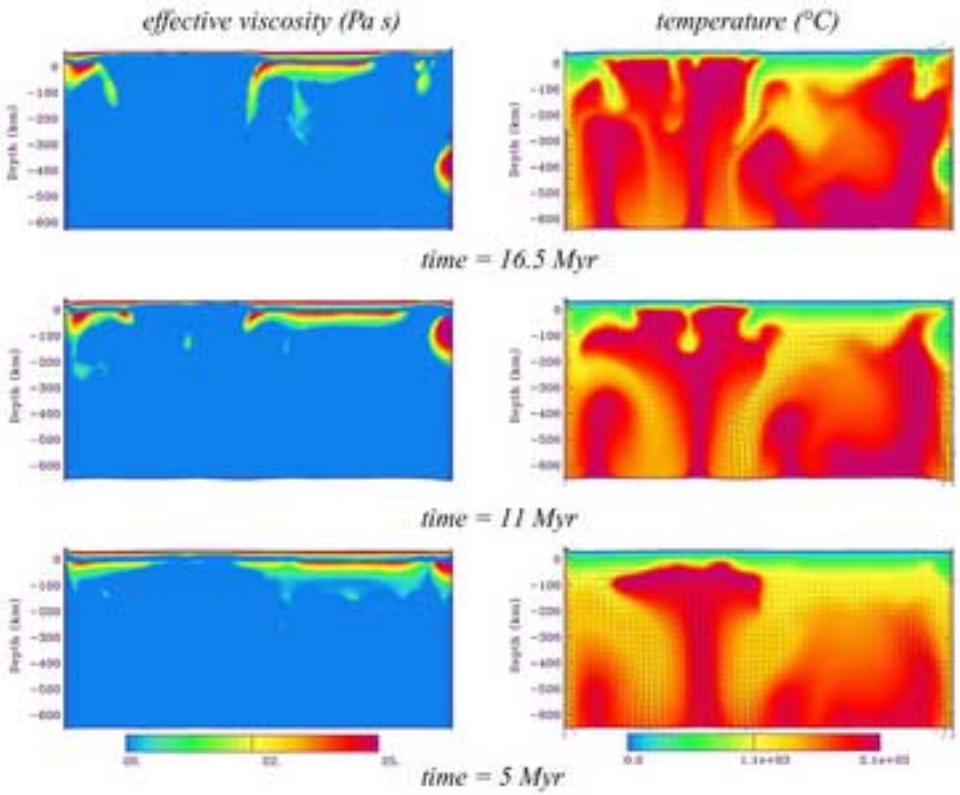

Figure 5b

Figure 6

Click here to download high resolution image

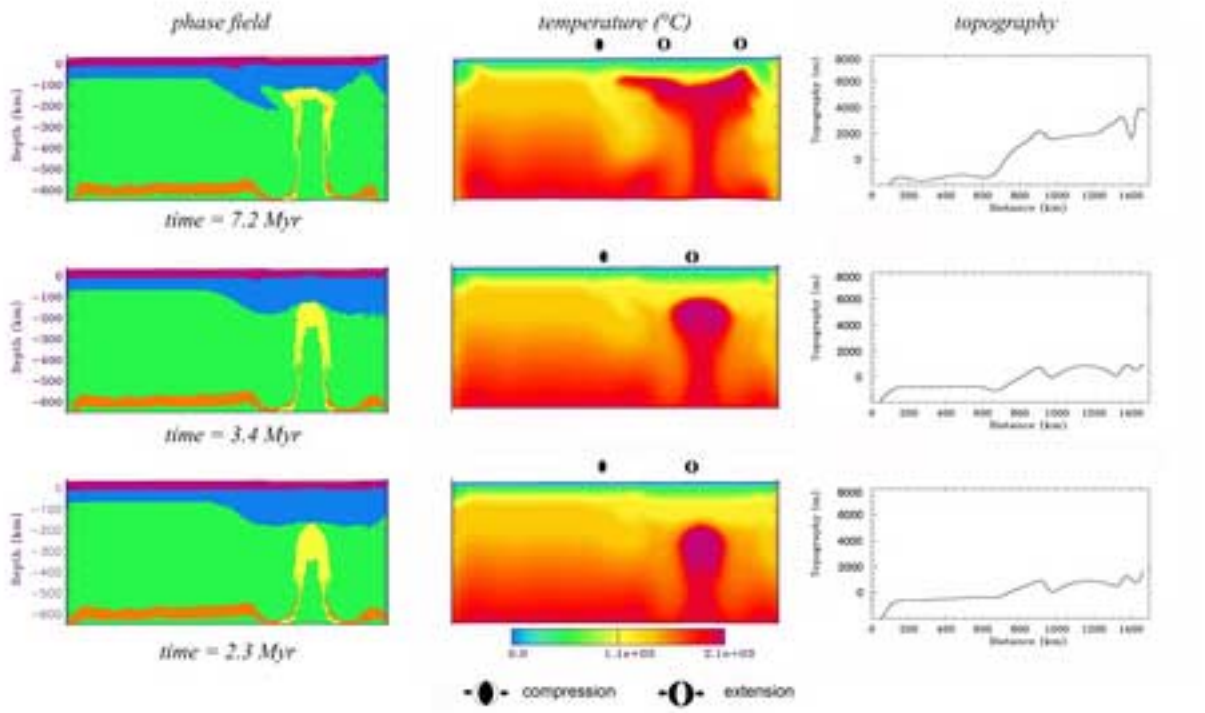

Figure 6

Figure 7a

Click here to download high resolution image

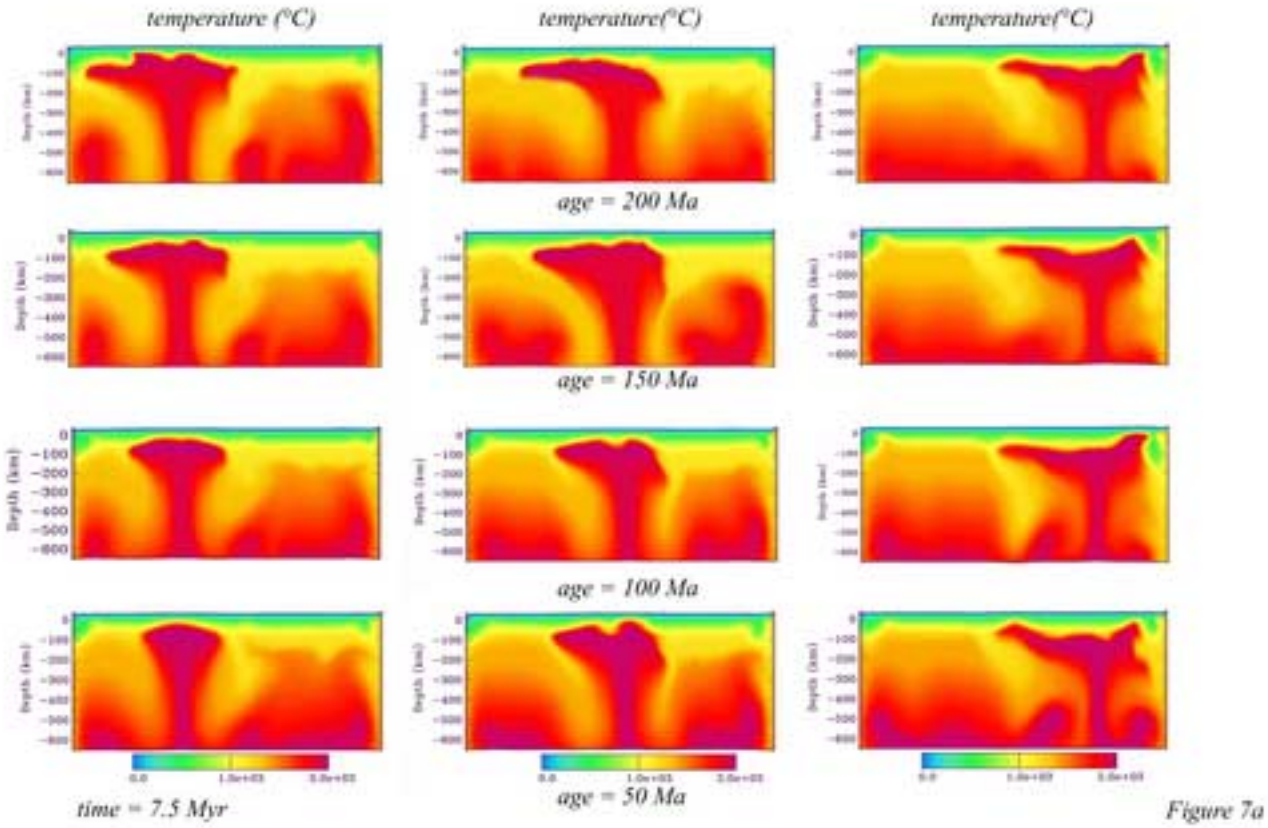

Figure 7a

Figure 7b

Click here to download high resolution image

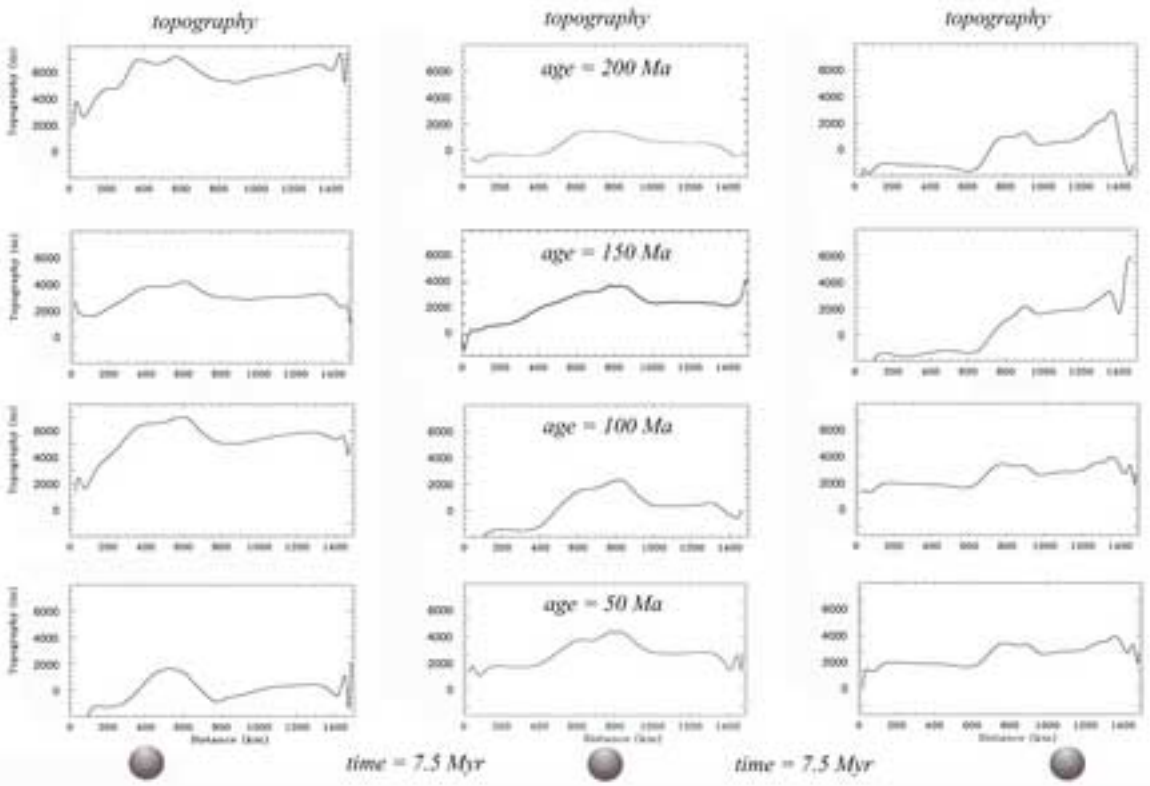

Figure 7b

Figure 8a

Click here to download high resolution image

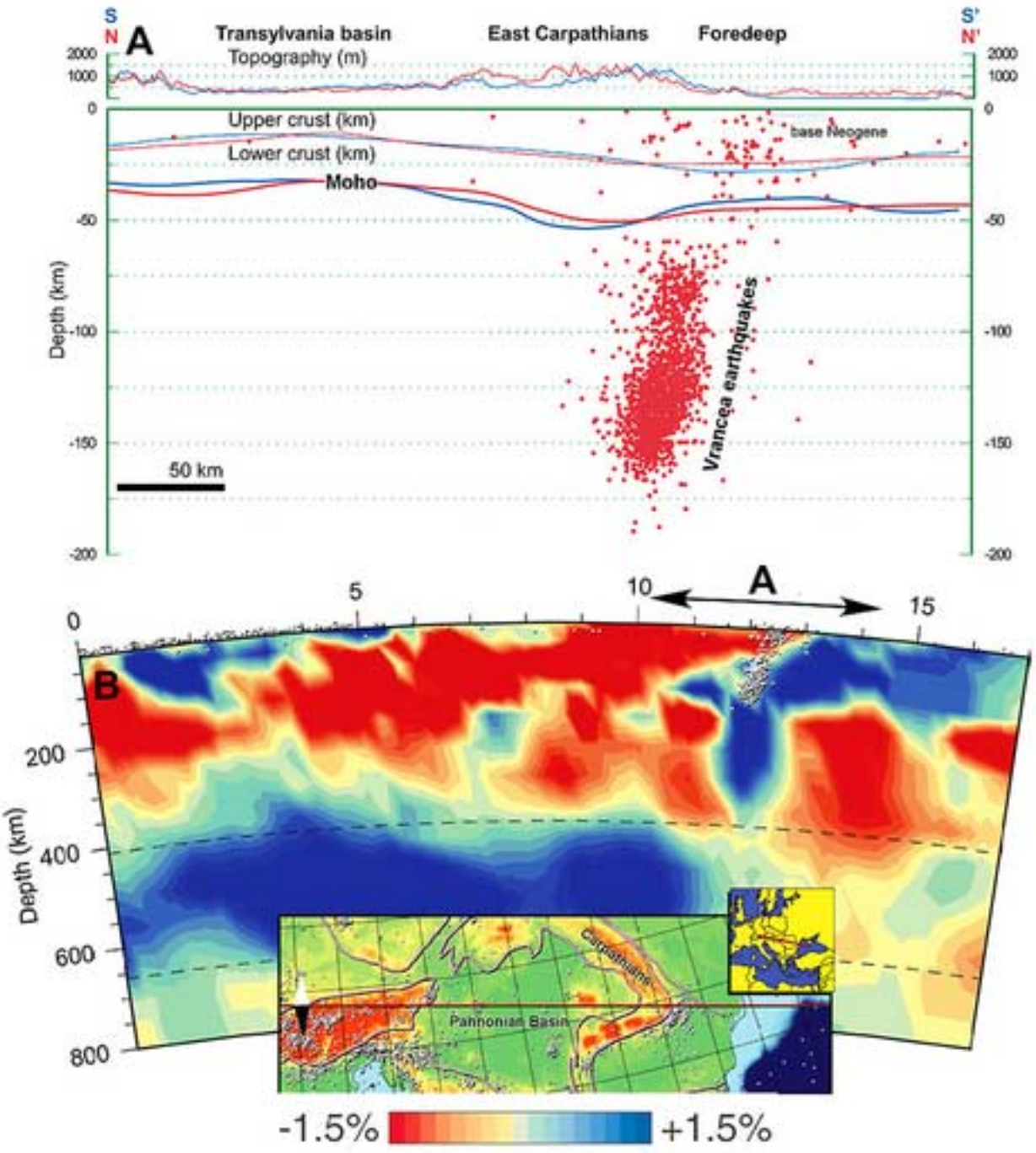

Figure 8a

Figure 8b

Click here to download high resolution image

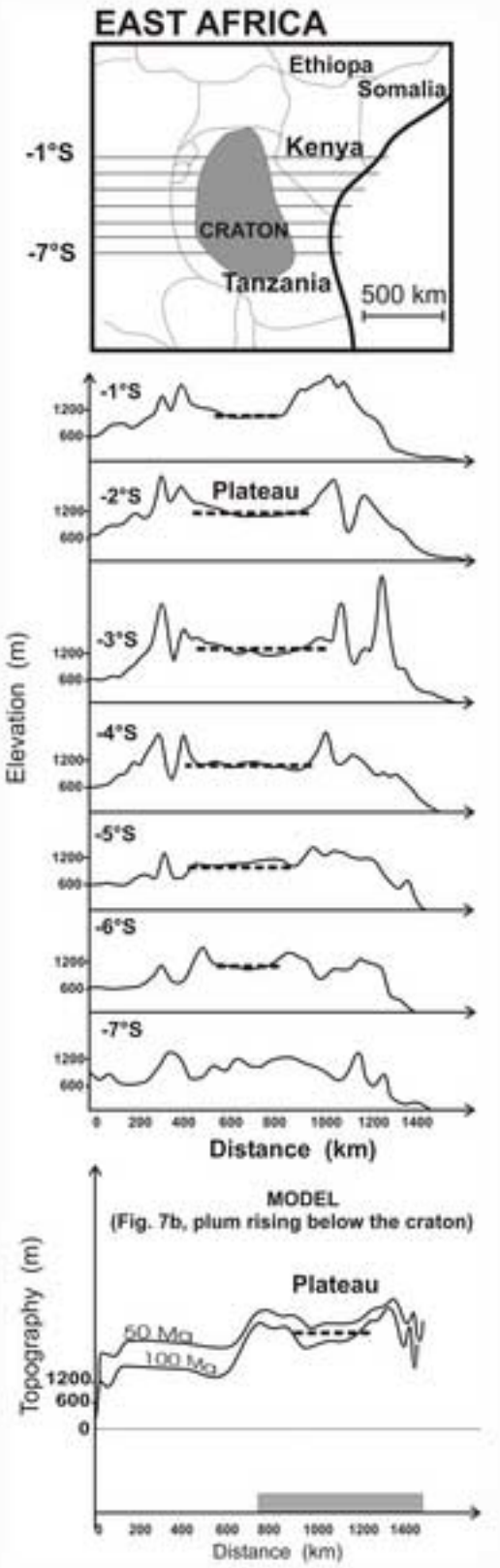

Figure 8b